Field Welding of Rails:
Failure Investigation of Thermite Welds
and Property Study of Electroslag Welds

Lisa Marie Cobb
B.Sc., Clarkson University
Potsdam, NY, 1987

A thesis submitted to the faculty of the

Oregon Graduate Institute
of
Science and Technology

in partial fulfillment of the
requirements for the degree

Master of Science
in
Materials Science

January, 1990

The thesis "Field Welding of Rails: Failure Investigation of Thermite Welds and Property Study of Electroslag Welds" by Lisa Marie Cobb has been examined and approved by the following Examination Committee:

Paul Clayton, Thesis Advisor
Professor

Milton R. Scholl,
Research Scientist

Jack H. Devletian, Professor

Acknowledgements

Thanks are due first to Paul, without whose patience and genuine concern this thesis might not exist. Many thanks also go to Milt, who was indispensable for his guidance throughout the project. Jack deserves acknowledgement for reviewing the thesis and offering valuable suggestions. The Wear Group as a whole with its unending support and good humor has made the experience a truly enjoyable one. Finally, many thanks to the Federal Railway Administration for providing financial support, and to Amtrak for the thermite welds.

For my Family.

Table of Contents

List of Tables

vii

List of Figures

ABSTRACT

The move toward continuously welded railroad rails in the
United States created a need for a welding method for use in the
field. Today the thermite welding process is used for joining
1/4-mile long "strings" of 39-foot rails electric flash-butt
welded at factory sites. Thermite welds have been found to be
less reliable than the factory made welds, with inherent defects.
As an alternative to thermite welding of rail, the Oregon
Graduate Center adapted the electroslag process to rail welding.
The current study examines both thermite and electroslag rail
welds; the former in the context of a failure investigation and
the latter as a mechanical property study.

A failure investigation was conducted on six thermite field
welds of which three were considered defective by Sperry Rail
Service's ultrasonic test car, and three acceptable. Sectioning
and radiography were performed. One weld was found to be grossly
defective, and the remaining five were found to have identical
defects. Inclusion and ferrite volume fraction estimates were
conducted on the welds, but no correlation was found with the
ultrasonic test results.

Eight electroslag rail welds were made with 136 lb./yd.
standard carbon rail. Tensile and impact tests, and inclusion

and ferrite volume fraction estimates were conducted on the weld metal. Wear and rolling contact fatigue tests were conducted on both the weld metal and the heat-affected zone. The tensile and impact properties were comparable to documented thermite weld properties and those of standard carbon rail. Wear and RCF properties were comparable to those of fully pearlitic rail steel; similar data for thermite welds is nonexistent. The volume fractions of inclusions and ferrite were comparable to those of the thermite welds received. It was concluded that the mechanical properties of electroslag weld metal are at least as good as those of thermite weld metal, and that the rolling/sliding resistance properties of the electroslag weld metal and heat-affected zone followed the same relationships with hardness as those of rail steel, and were at least as good in this area.

INTRODUCTION

Railway transportation became vital in the United States following the Civil War when the rails became standardized and free interchange among the railroads was established [1]. Since the 1860's, speeds and loads have increased dramatically from 30-ton cars travelling at an average of 18 mph [2] to today's 100-ton cars travelling at speeds of 70 mph. Already some 125-ton cars are in existence on limited lines, with a gradual change to these heavier vehicles anticipated in the next few years.

The first steel rails were rolled in 1865 [1,3] and were joined by bolted fishplate connections, as shown in Figure 1. Continuously Welded Rail (CWR), defined by the American Railway Engineering Association (AREA) as "a number of rails welded together in lengths of 400 feet or longer" [3] has, since the early part of this century, been a goal of the railroads. The miles of welded track laid has been recorded by AREA since 1933. The data reproduced in Table I reflects the trend in the industry of gradually installing more CWR in an effort to reduce joint

failures and lower maintenance costs [1].

The move toward CWR started as heavier loads and faster speeds on the railways resulted in the need for a more reliable joint. The faster, heavier trains became necessary due to competition from the developing trucking industry. The introduction of diesel and electric locomotives made hauling heavier loads at faster speeds possible. The new cars put much higher bending and impact loads on the old bolted joints, which then cracked at the bolt holes and showed increasing rail end batter. The railroads began replacing some of the bolted connections with factory-made welds and the mills began rolling rail of heavier cross section. The very first rails rolled in 1865 were of the same basic T-shape as today's rails but with a weight of only 50 lb. per yard. Common sections now in use range from the lighter-duty 115 lb. per yard rails to the most common 136 lb. per yard and 140 lb. per yard rail [3].

In the 1920's it was apparent that much lower maintenance costs for welds justified the higher initial investment for installing CWR. Gas-pressure welding initially gained favor as a factory rail welding method around 1937. Standard 39-foot rails were welded in factories into longer sections ("strings") which were then joined in-track by fishplates, although some experiments were conducted with in-track gas-pressure welders. By the 1950's, electric flash-butt welding had begun to displace gas-pressure welding for factory-made welds, and thermite welding

was being used increasingly as an in-track welding procedure in the U.S. Today thermite welding is used exclusively. [4]. Gas-pressure welding gave way to electric flash-butt welding as a factory process, and while some equipment is still in use, no new gas-pressure welders have been installed since 1955 [5].

RAIL WELDING PROCESSES

Electric Flash-Butt and Gas-Pressure Welding

Factory electric flash-butt and gas-pressure welding processes use electrical energy and gas heat, respectively, to heat the rail ends in preparation for joining. The electric flash-butt (EFB) welding process, shown schematically in Figure 2, uses high current flow (20,000-100,000 Amps at 5-10 V) to preheat the rail ends. At the same time, they are brought together with a force of 50 to 65 tons and separated up to 20 times to "flash" off rough spots at the ends and to bring the temperature to 1750° to 2000°Fahrenheit. When the desired temperature is reached and melting occurs the rails are brought together one final time, forcing the molten material out of the contact area so that only a heat-affected zone remains [4]. The resulting upset is then sheared (usually automatically) from the rail. This process requires no cleaning of the rails ends or post-weld heat treatment.

Gas-pressure welding, on the other hand, requires clean rail ends. The rails are cut simultaneously on opposite sides of the saw blade to ensure alignment, then they are cleaned and welded immediately. The aligned rail ends are heated to 2500°F by oxy-fuel torches, then forced together only once. No melting occurs in the process. After cooling to 900°F, the resulting welds are heated again and normalized at a temperature of 1550°F with oxy-fuel torches. The reason electric flash-butt welding gained favor over gas-pressure welding was because EFB does not require expensive and time-consuming rail-end cleaning or post-weld heat treatment. Gas-pressure welding is also slower and gas-pressure welds were found to fail on average three times more often than EFB's.

Thermite Welding

Thermite welding was invented in 1896 when Hans Goldschmidt first used an oxidation-reduction reaction of a metal oxide in combination with aluminum [6]. As a result of the high free energy difference between the metal oxide and the aluminum the reaction, once initiated, proceeds to completion in a highly exothermic manner. The reaction products are aluminum oxide and the de-oxidized metal, both in liquid form, separated by their different fluid densities. Since the reaction produces large amounts of heat, Goldschmidt suggested that it could be used for welding and helped to develop the process now known generically

in this country as thermite welding, also known as thermit and
aluminothermic welding. The development of this process was
largely made possible by the preceding development of
electrolytic separation of aluminum in the late 19th century.
This greatly reduced the cost of aluminum required for the
process. For example, in England in 1889 aluminum cost 3000
pounds per ton. Seven years later, it cost only 163 pounds per
ton. [7]

Industry has found a number of uses for the thermite process
[7,8]. It is used for production of carbon-free metal alloys
which may otherwise be difficult to melt, such as chromium,
manganese, and alloys of FeCr, NiCr, and FeMn. Other uses are as
hot-topping compounds in the steel-making and foundry industries
to eliminate piping defects, and for destruction or demolition
when blasting or explosives can not be used. Of course, it is
also used for joining. Major uses include the mechanical joining
of reinforcement bar in large concrete structures and welding
pipelines in remote areas.

The thermite process as it relates to the joining of steel
products uses the following two common thermite reactions:

$$Fe_2O_3 + 2Al \rightleftharpoons 2Fe + Al_2O_3 + 182 \text{ kCal}$$

$$3Fe_3O_4 + 8Al \rightleftharpoons 9Fe + 4Al_2O_3 + 719 \text{ kCal}$$

The first is used in the Goldschmidt process (Orgotherm brand)
and Calorite and Boutet processes. The second is used in the
U.S. Thermit process [4]. The welds investigated in this study

were made by Amtrak welders using the Boutet process. Figure 3 shows a schematic of the process set-up. The reaction takes place in a refractory-lined crucible which is tapped at the bottom. The liquid steel formed in the thermite reaction flows into the weld mold around the rail ends.

The aluminum and iron-oxide used in thermite welding are in powder or granular form contained in a pre-mixed bag. Other ingredients are added to slow down the reaction which could otherwise be unmanageably violent. Non-reacting constituents, such as ferroalloys, are added to alloy the steel and to reduce the reaction temperature. Too high a reaction temperature can cause vaporization of aluminum particles; too low and the steel will not separate quickly enough from the slag and retain enough heat to flow freely into the mold.

Among the factors considered in designing an optimum thermite mixture is the aluminum content. Excess aluminum can cause weld embrittlement by encouraging the formation of Type II Manganese Sulphide films at the grain boundaries. A small amount of aluminum, in addition to that which is stoichiometrically required for the reaction, is desirable to prevent oxygen from iron oxides reacting with other elements in the mix or with the reaction vessel itself [6]. Insufficient aluminum can cause hot shortness due to steel-making constituents reacting with the iron oxides.

Finally, the size of the aluminum particles is also of importance. If they are less than 10 um diameter the reaction proceeds very fast because of the high surface area to volume ratio. The violence of this heightened reaction rate has a tendency to blow the powdered aluminum out of the reaction crucible. The resulting shortage of aluminum leads to excess iron oxide that can not be completely reduced to iron. This in turn can lead to iron oxide inclusions in the weld. However, if the aluminum particles are larger than 1000 um in diameter, the reaction proceeds slowly, causing a low peak reaction temperature and a loss of fluidity of the molten metal [9,10]. The slag may not have enough time to separate from the molten metal.

All of the thermite constituents must be balanced to achieve full slag separation, a manageable reaction, desired fluidity of metal for proper mold filling, and optimum metallurgical properties. The complexity of this problem enables thermite weld mixture compositions to remain proprietary.

In addition to determining a correct mixture for the welding reaction, proper procedures must be carefully followed to ensure that the resulting thermite weld is of good quality. The Amtrak Joint Elimination Procedure [11] is used by the national passenger railway's welders to obtain a good quality quick preheat Boutet thermite weld. The procedure is outlined in detail in Appendix 1.

The crucible is first checked for cracks, then preheated. The rail end temperature is recorded, the gap between the rail ends is set at approximately 1-1/4 inches, and the rail ends are cleaned with a wire brush. The rails are cambered, or "crowned", as shown in Figure 4. The molds are then inspected, applied, and sealed to the rail ends with refractory cement. Next, the reaction crucible is filled with one measured bag of the thermite weld mixture and swung out to the side of the weld area while the rail ends and attached mold are preheated with an oxy-fuel torch. When the desired rail end temperature (as judged by the color of the rails seen through specially designed glass) is reached, the crucible is moved into position and the charge is ignited. An automatic tapper, consisting of layers of metal which melt successively, controls the release of the molten material from the bottom of the crucible. After the weld has cooled for a few minutes, the mold is removed. The weld is then finish-ground and visually inspected.

The procedure outlined by Amtrak is very specific and the instructions are meant to be carried out in detail to prevent operator error. Operator error may take several forms. Molds, mixtures, and crucible must be handled carefully and attention must be paid to their appearance and protection. Moisture on the rails or in the weld mix (even if it has dried) can lead to weld porosity. The molds, crucible, and rail ends must be clean, as any debris present can become entrapped in the weld. If the

molds are jostled or not properly covered, sand or other material can fall into them, again becoming entrapped in the weld metal. Too large a rail end gap can lead to the weld running short of material. Insufficient preheat can lead to lack of fusion, and/or detrimental microstructure heat-affected zone (HAZ). Too long a preheat can cause melting of the rail ends which leads to oxide inclusions. An uneven preheat can lead to lack of fusion on one side of the weld. The crown must be correct before welding or the resulting uneven running surface can lead to rail batter. In finishing the weld, grinding or otherwise straining the weld prematurely can cause hot tears inside the weld.

The thermite welding procedure has, therefore, an inherent susceptibility to defects. Thermite welds have a much higher failure rate than either electric flash-butt or gas-pressure factory welds. As a result, there is interest in developing a field welding process that can be more easily automated. In-track flash-welders have been used for new track installations [4,12]. However, they are not entirely suitable for small jobs because they require a rail car for transportation. The thermite weld operation can be loaded onto a truck equipped with rail wheels (a "high-railer"). Moving the operation from site to site does not tie up valuable rail time since the truck can travel on the highways. Any new method must be economically competitive with thermite welding, proven to be more reliable and equally portable. Electroslag welding of railroad rails has been

explored to this end.

Electroslag Welding

The electroslag welding process (ESW) was developed in the
Soviet Union in the 1950's. The American Society for Metals
(ASM) Committee on Electroslag Welding defines ESW as

> "a process that uses the heat generated by passing an
> electrical current through a pool of molten slag (flux) to
> melt the edges of the joint (base metal) and a filler wire
> (electrode). The electrical resistivity of the molten slag
> continuously produces the heat necessary to continue the
> welding process" [13].

Thus, although ESW is often grouped with arc-welding processes,
it is (except for starting) an arc-less process. It is a single-
pass weld used mainly on thick (over 3/4-inch) cross-sections,
commonly of steels and other iron-based alloys. Electroslag
welding can be used on smaller components but it has a sound
economic advantage over arc-welding processes on large cross-
sections since it uses only a single pass. A schematic of the
ESW set-up is shown in Figure 5. The slag is formulated so that
it floats with a liquid density less than that of the molten
metal. It is highly resistive and converts the electrical energy
into heat energy to melt the base metal and the electrode wire.
It may also melt the wire guide tube. As the wire is fed into
the weld, the volume of weld metal enclosed by the copper

retaining shoes increases, and the weld progresses vertically.

One type of electroslag welding uses a consumable guide tube; in the other the guide tube is not melted. In the latter type, the welding equipment moves upward to keep the guide tube from melting. The consumable guide tube method, with its stationary guide tube, has been used almost exclusively by the Oregon Graduate Center (OGC).

In starting an electroslag weld, the guide tube is positioned about 1-1/2 inches from the bottom of the weld joint. An arc is struck on a starting block which maintains electrical contact with the base plates. The starting area is covered with a powdered flux consisting of oxides of calcium, manganese, silicon, aluminum, and others, and calcium fluoride [14]. The flux, when melted, is designed to provide the desired electrical resistivity, viscosity, and temperature of the molten slag. The arc initially melts the flux but rapidly extinguishes as the molten flux volume increases. The current is then carried by the highly resistive slag which converts the electrical energy into heat energy by electrical resistance (I^2R) heating. The temperature of the slag bath is approximately 3000°F and it melts the guide tube and faces of the base metal, given appropriate operating conditions. No edge preparation is necessary because of the cleansing action of the molten slag, which collects the lighter-density impurities. Flame-cut edges may be used with no damage to the properties of the weld metal or the heat-affected

zone. The external profile of the weld is determined by the shape of the water-cooled retaining dams, or shoes.

This welding process has been adapted for railroad rail welding as an alternative to thermite welding because of its reported inherent weld metal cleanliness, its potential for automation, and its portability. This adaptation was conducted by OGC, with funding from Southern Pacific Railroad which now holds the patent. The process has remained in the experimental stage for the last ten years because of lack of further funding and has not yet been fully developed for use in the field.

PROPERTIES OF RAILROAD RAIL WELDS

The properties of thermite welds have been studied by several investigators [4,7,15-19]. Generally, thermite welds exhibit an ultimate tensile strength (UTS) of 100 to 160 ksi (680 to 1100 MPa) and a yield strength of 60 to 110 ksi (400 to 700 MPa), with two to six percent reduction-in-area (RA). The weld metal hardness generally varies from 20 to 32 HRc (230-300 Brinell) for a standard carbon rail weld. The hardness varies with composition, preheat time, cooling rate and position in the weld. Thermite weld metal Charpy V-notch (CVN) impact energies at room temperature range from one to three ft-lbs [20].

Electroslag welds made from comparable rail steel of .65%

carbon have an ultimate tensile strength of 118 ksi (805 MPa) and a yield strength of 75 ksi (515 MPa), with 1.6% RA and 2.5% elongation for a gage length of two inches. These welds showed a weld metal hardness of 22 to 25 HRc (240-255 Brinell) and standard CVN values of an average of 2 ft-lbs. Dynamic fracture toughness (K_{1d}) values had an average of about 40 ksi(in)$^{1/2}$.

Gas pressure and Electric Flash-butt weld properties have been measured by slow-bend and rolling-load tests. These tests attempt to duplicate actual rail loading, and cannot be directly compared with the mechanical property data for electroslag welds. Rolling load and slow-bend tests have also been conducted on thermite welds. For four-point bending with a four-foot span supported at the ends and loads at points six inches from the weld, the Association of American Railroads (AAR) recommends a minimum deflection of 1.5" at failure and a modulus of rupture of 140,000 psi. Most factory welds pass this test, and most thermite welds do not. This test has been used by the railways while the slow-bend and three-point loading drop tests are used regularly to check weld quality at the welding plant. [19,21,22]. Generally, the flash-butt welds out-perform thermite, EFB, and gas-pressure welds on both tests. The gas-pressure welds do equally well on the rolling-load tests, and are slightly inferior in the slow-bend test. Thermite welds perform less well than the gas-pressure welds [4]. Rolling load tests are being conducted on electroslag rail welds by AAR. The results are not yet

complete, however, initial results indicate that the electroslag welds produced so far do not compare favorably with the thermite welds.

RAIL WELD RELIABILITY

In the U.S., electric flash-butt and gas-pressure welds have been found to have relatively good reliability. In 1970, in new rail there were .004 failures per 100 weld years (a weld year equals the number of failed welds times the average age of those welds) of electric flash-butt welds, and .009 for the gas pressure welds [21]. The thermite welds had a failure rate of about 100 times the average of the others, at .364 failures per 100 weld years, Figure 6. These data show that thermite welds fail sooner than factory welds, having a high incidence of "infant mortality".

Weld failure data was voluntarily reported by the railroads, along with the miles of CWR laid, to AREA until 1979. Railroad reorganizations, acquisitions, and the resulting confusion made gathering the failure statistics very difficult, and the railroads gradually stopped reporting them. The partial data was considered to be of "little or no value" [23]. In 1987 AREA completely stopped collecting these data; the 1979 report on CWR data is the last. That report included data on the number of

welds made, but did not include data on weld failures. The 1970 weld failure report appears to be the last published in the U.S.A.

British Rail statistics [22] show that thermite welds fail approximately 10 times more often than EFB's, as seen in Figures 7a and 7b. The BR analysis did not, however, take into account the age of the failed welds, so they may not be directly compared to the U.S. data. They do show, however, that thermite weld failure rates are significantly higher than factory weld failure rates in Britain as well. The peak in the EFB curve in 1980 was attributed to chiseling the weld upset, a practice that was discontinued when automatic weld trimmers were introduced.

CAUSES OF WELD FAILURE

The main cause of failure of gas-pressure welds has been found to be lack of fusion from mill scale entrapment or acetylene carburization on the rail ends leading to a carbon-rich layer which forms hard structures on cooling. The sudden loss of the preheater flame can cause both defect structures, and its occurrence depends on the balance of gases in the flame. Excessive acetylene leads to carburization; excess oxygen can lead to oxidation at the surface. Oxides on the rail end surface can become entrapped and become sites for crack initiation, or

lead to lack of fusion. Other failure modes reported are [4] insufficient upsetting and lack of parallelism which cause high stress concentrations in the weld region. Commonly reported causes of failure in electric flash-butt welds are electrode burns on the rail base which lead to the formation of brittle martensite, and iron-oxide inclusions in the weld fusion line from flash particles in the weld zone after upsetting, and lack of fusion [24-27]. The last two can be caused by too short a weld cycle [4]. Other causes of failure reported are insufficient grinding, hot tearing from straining the weld before it is fully cooled, and martensite formation from over-zealous profile grinding.

Lack of fusion at the weld line resulting from improper preheat has been identified as one cause of failure in thermite welds. Porosity in the weld, entrapment of oxides from sand molds (in the head, web, collar, and foot areas), and formation of martensite from the grinding operation have also been identified as initiation sites for fracture [24,25,28,29].

The current study attempts to expand the knowledge base of the thermite field rail welding method in the United States by incorporating a failure analysis of thermite welds in an effort to determine the possible causes for weld rejection based on ultrasonic evaluation. The properties of electroslag rail weld metal have been determined by dry rolling/sliding wear, lubricated rolling contact fatigue, Charpy and tensile tests.

This work is therefore presented in two sections. The first concerns the thermite weld failure investigations and the second encompasses a study of electroslag rail weld properties.

EXPERIMENTAL PROCEDURE

THERMITE WELD FAILURE ANALYSIS

Sectioning and Macroscopic Examination

The thermite welds examined were provided by Amtrak via the Federal Railway Administration (FRA). The information received on the six thermite welds is given in Table II. Three of the welds passed ultrasonic evaluation and three failed. After visual inspection, all six welds were band-sawed down the vertical longitudinal axis. The shape of the heat-affected zones were examined by etching sections with 10% nital (10 mL nitric acid in 100 mL ethanol) and tracing the resulting outline, as shown in Figures 8a-8c. The longitudinal section was then cut in half, transverse to the rail axis and sections were taken in the weld zone at the head and foot of the rail for metallographic examination, Figure 9.

Radiography

Welds were radiographed after initial sectioning by Pittsburgh Testing of Portland, OR. The welds were placed flat on the cut longitudinal surface and were viewed with the x-ray

source perpendicular to the rail. A double film technique was used to compensate for the variations in section thickness. The radiographs could then be viewed either together or separately, making the defects easy to see with proper illumination. Defects indicated by the radiographic analysis were cut out, mounted, and examined to determine their possible causes.

Chemical Analysis

Chemistries of the thermite welds were determined by spark spectrographic analysis, on the metallographic sections taken from the head of the weld.

Metallography

Sections were polished and inclusion volume fractions estimated on unetched specimens using the standard practice ASTM E 562 [30]. The procedure involves placing a transparent grid over an optical microscope ground glass viewing screen at a magnification that projects the constituent being counted as approximately one-half the distance between the points. When the constituent covers an intersection of the grid, this counts as one "point"; one-half point if the constituent just touches the intersection. This is repeated for a minimum of 30 fields chosen at random. The following equation is then used to determine the

volume fraction of the constituent:

$$\text{Volume Fraction} = 1/n * \sum_{i=1}^{n} P_{P_i} +/- \text{C.I.}$$

where n equals the number of fields, P_{P_i} equals point count on the ith field divided by the total number of grid points times 100%, and C.I. equals 95% confidence interval. A two-millimeter square, 30 by 30 grid was used at a magnification of 200X for 30 fields for each specimen for the thermite weld inclusion measurements.

Metallographic specimens were etched with two-percent nital and the same manual point count procedure employed to estimate the volume fraction of proeutectoid ferrite. The ferrite showed up on an etched specimen as white areas at the prior austenite grain boundaries and often around inclusions.

Microhardness

The microhardness of each section was measured using a Knoop diamond indentor with a load of 500 grams. An attempt was made to use a Rockwell "C" hardness tester on the welds, but there was considerable scatter in the data for any given weld. Knoop microhardness was found to be more consistent. Eight to twelve measurements were taken in the weld zone, averaged and converted to Brinell scale for comparison with other published rail hardness data.

ELECTROSLAG WELDS

Welding Equipment

The electroslag welds were made with Nippon Kokan 136 lb/yard head-hardened standard carbon rails, all from the same heat. Using the fixture shown in Figure 10 designed for welding rails in the laboratory, four- to eight-foot lengths of rail were mounted and welded using the ESW procedure developed at OGC for welding railroad rail [14,31,32].

The electroslag rail welds were made using two Hobart Model PC-750 constant voltage power supplies connected in parallel and a Hobart dual wire feeder. Two high carbon 3/32" diameter wires, Page AS-65, were used simultaneously with welding parameters of 32 volts and approximately 1100 amps. The consumable guide tube was of a special plate design, Figure 11, constructed such that the top half was made of high carbon steel (cut from standard carbon rail) while the rest was mild steel.

Electroslag Welding Procedure

The detailed welding procedure which follows in detail is that adapted by OGC for the welding of railroad rail [14,31,32]:

1. The rails were aligned with a 1-1/4" gap between rail ends. No joint preparation was needed other than

removing any grease or loose debris from the cut ends. The wire feeder was then clamped onto the rail, and the power leads, ground leads, and wire feeder power were connected.

2. The ceramic liner was placed in the starting block, covered with a formed steel plate for electrical conductivity, and the entire starting block assembly, Figure 12, was inserted under the rail base centered on the gap, positioned and clamped in place. Two hundred grams of Hobart PF-201 electroslag welding flux was distributed in the starting trough.

3. The consumable plate guide tube was inserted and aligned. Consumable ceramic insulators were placed between the plate guide tube and the rail ends to prevent shorting.

4. Water-cooled copper shoes, Figure 13, were clamped to the rail and carefully centered on the joint gap and guide tube. Next, copper run-out blocks were aligned on top of the rails, and the gaps between the copper shoes and rails were sealed with refractory cement.

5. The power supplies were turned on and the weld started with one wire. Once the arc had stabilized, after about 30 seconds, the second feed wire was started. After both arcs had stabilized and the slag bath was established, an additional 200 grams of PF-201 flux was added. As the weld proceeded, another 100 grams of flux was added. Cooling water was added two minutes after the weld initiation and the flow adjusted to maintain an outlet water temperature of 120-180°F, for an inlet temperature of about 55°F.

6. The weld was terminated when the slag bath reached the top of the copper run-out blocks, approximately 14-16 minutes after weld initiation. This provided a weld metal run-out about one to one- and one-half inches high. Cooling water flow was maintained until the cooling shoes were removed from the weld, about five to ten minutes after weld termination. The weld temperature is below 1000°F at this time.

Sectioning

A special fixture was used to position the welds for sectioning on a StartRite horizontal bandsaw. Slabs were sectioned from the weld for tensile bars, CVN specimens, and Amsler rollers for wear and rolling contact fatigue (RCF)

specimens. Diagrams showing specimen placement appear in Figures 14 and 15.

Special care was taken in the machining of all specimens to ensure proper orientation. Standard one inch gage length, 1/4"-inch diameter tensile bars and standard sized CVN specimens were machined. To obtain weld metal properties, the failure of the tensile bars had to occur in the weld metal. This was achieved by polishing the bars to an hour-glass shape four- to six-thousandths thinner in the center of the gage length. The Charpy V-notches were broached into the specimens so that the notch ran along the weld centerline, and the crack was driven in the direction of grain growth, as shown in Figure 16. It has been found that driving the impact fracture parallel to the growth direction of the grains in the electroslag weld metal gives the most conservative test results [14]. Rollers for wear and RCF tests were machined as shown in Figure 17.

Chemical Analysis

Chemical analysis was performed on a spark-emission spectrometer for all eight electroslag welds. The weld metal chemistry was analyzed from a specimen surface at the very top of the rail head using a section of the run-out at the top of the weld.

Metallography

Optical metallography was performed on a Nikon Epiphot microscope. Longitudinal sections were examined from the center of the head of the rail oriented perpendicular to the base of the weld. The welds were characterized in the same manner as the thermite welds. The volume fraction of inclusions and the volume fraction of ferrite were estimated using the same parameters as used for the thermite welds except that the magnification of the fields for inclusion counting of the electroslag rail welds (ESRW's) was 400X instead of 200X. The reason for the change in magnification is that the standard practice, ASTM E 562 discussed previously, states that the grid size on the viewing screen shall be about twice that of the constituent in question. The necessity for a higher magnification shows that the inclusions in the thermite welds are larger than those found in the electroslag welds.

Ferrite volume fraction was estimated on the ESRW's using the same practice, but again at a magnification of 200X instead of 400X. At this magnification, the percentage of error, defined by ASTM as the 95% confidence limit divided by the volume fraction, was twice that for the thermite measurements where the 2mm square grid was used. Two different circular grids were then tried to see which indeed was the best grid configuration and magnification. Four trials were conducted on as many thermite welds at 400X (since the results were known to a greater degree

of accuracy) using the two different circular grids. Neither gave results with less error than the square grid at 400X magnification. The ferrite volume fractions were again estimated for four <u>electroslag</u> welds at 200X and at 400X, using the square grids. At 400X the results showed as much scatter as in the results at 200X. It was concluded that the ferrite is not as randomly dispersed in the electroslag welds as it is in the thermite welds. Thereafter, all remaining electroslag weld ferrite volume fractions were estimated with a 2mm square grid at 400X for the sake of consistency with the thermite welds, accepting the scatter in the electroslag results.

Tensile Testing

Tensile testing was performed on an Instron Model 1335 Universal Testing machine with a 120 kip capacity. Tests were run and data acquired using computer control of the testing machine. The computer monitored and controlled the load rate and at the end of each test calculated the ultimate tensile strength and the 0.2% offset yield strength. The percent reduction-in-area was measured on the fractured sample. After testing, the fracture surfaces were examined in a scanning electron microscope (SEM).

Impact Testing

Charpy V-notch specimens were tested in a Tinius-Olsen Instrumented Impact Pendulum Machine. Though the tup on this machine was instrumented, only the dial energies were recorded. All testing was performed with specimens at room temperature. After testing the fracture surfaces of the Charpy bars were examined in the SEM.

Wear and RCF Testing

Wear and rolling contact fatigue (RCF) tests were performed on an Amsler twin roller machine, Figure 18, employing specimen geometries shown in Figure 17. Wear tests were performed at contact pressures of 1220, 900, 700 and 500 N/sq.mm with a 35% slide/roll ratio. The latter represents the differences in velocities of the two rollers and was determined from the following equation [33]:

$$S/R \text{ ratio} = \frac{2(1.104 * D_2 - D_1)}{D_1 + 1.104 * D_2}$$

where D_1 and D_2 are the upper and lower roller diameters, respectively. The top roller had a diameter of 35mm; the bottom roller 45.01mm. The contact pressure was calculated from the following equation [34,35]:

$$P_o = F_N * \frac{E}{(1-v^2)} * \frac{D_1 + D_2}{l_c * D_1 * D_2 * pi}$$

where P_o is the contact pressure, F_N is the normal force, E is the elastic modulus of the material (210,000 N/sq.mm was used), v is Poisson's ratio (0.3 was used), l_c is the contact width, and D_1 and D_2 are the same as in the previous equation.

Wear tests were performed using top rollers from the rail welds and all the bottom ones from a single Class "C" wheel. The specimens were weighed and their diameters measured. They were run at 200 rpm for 100 or more revolutions or until there was measurable wear, then removed, re-weighed and the diameter re-measured. The Amsler wear test matrix of samples and contact pressures is shown in Table III.

RCF tests were undertaken to characterize the rolling contact fatigue behavior for the electroslag rail weld metal. Tests were also run to develop the linear portion of the S-N curve for the electroslag weld metal. Rolling contact fatigue tests were run on samples taken from analogous positions to the wear test rollers, and were run on the same wheel material. All tests were run at 400 rpm with water lubrication, so that no measurable wear was generated. Tests were started and allowed to "run in" until the vibration level of the machine stabilized, and then a trip indicator (accelerometer) was set to shut off the machine at a given level of vibration. This trip level setting stopped the test at failure. The number of cycles and the initial work counter value were recorded at the start of the test, and the work trace was recorded. The RCF test matrix is

shown in Table IV.

Heat-Affected Zone Measurements

The HAZ profiles of the electroslag welds were measured by taking sections parallel to the rail base, as shown in Figure 19. Sections were taken from the same location in all eight welds. The welds in this study were made in the same manner as the ones in a previous study [14,31,32], therefore any HAZ abnormalities should be detected by comparing these data with the previous work. These sections were etched, surface ground, and hardness traverses taken. The hardness was measured using a Rockwell "C" hardness tester spacing the indentations approximately five millimeters apart.

RESULTS

THERMITE WELD EXAMINATION

Initial Examination and Sectioning

Complete information on the thermite welds received can be found in Table II. Three welds, TW-1, TW-2, and TW-6, were judged defective by Sperry Rail Service. All of the thermite welds were in track for some period of time; the time between installation, inspection and removal from track is unknown. Only weld TW-6 had visual defects, three holes approximately 1/4" in diameter on the rail running surface, and was presumably removed immediately after manufacture. All of the welds had a coating about 1/8" to 1/4" inch thick of refractory material from the thermite molds on the web area, which obscured possible defects, Figure 20. Of the three rejected welds, defects were found in welds TW-2 and TW-6 by sectioning. Weld TW-6, Figure 21, was found to have large voids due to shrinkage or gas porosity (approximately 1/4" by 1/2" by 1") spaced approximately 1/4" apart and found throughout the weld metal. Weld TW-2 had a 1" by 1/4" by 1/2" defect positioned on the centerline of the weld

toward the outside of the collar area. The orientation of the defect is shown schematically in Figure 22; a photograph of the actual defect is shown in Figure 23.

Radiography

Radiography was carried out first on Weld TW-1 to find the source of the ultrasonic indications. A defect was found on sectioning consisting of a hole approximately 1/8" across in the weld head area, shown as "A" in Figure 24. It was considered to be too small to have been detected ultrasonically. Radiography revealed indications in three other areas, also shown schematically in Figure 24. Defects "B" and "C" were uncovered by sectioning after radiography indicated the location for band-sawing. Defect "B" was found in the collar of the weld, just under the head (similar to the defect found in weld TW-2 on initial sectioning). It was approximately one inch long and 3/8" wide and deep, consisting of a cluster of roughly shaped voids. Defect "C" was found close to the centerline of the weld and was similar in nature to defect "B". It measured approximately one-half inch in diameter. A fourth defect, "D", which was not evident on the radiographs, was found by chance during later sectioning . It was also similar to the defect in weld TW-2 and the defects "C" and "D" of weld TW-1.

All remaining welds, with the exception of weld TW-6, were then radiographed to closely examine the differences between the

accepted and rejected welds. Weld TW-6 was not extensively
sectioned or radiographed since it was obviously defective. All
of the welds exhibited the defect initially found in weld TW-2,
and later in weld TW-1 (defect "B") in the collar. It typically
appeared as a cluster of voids, 1/8" to 1/4" wide and ranging in
length from 1/2" to 3/4". Dendrites were observed in the voids
when examined in the scanning electron microscope. Figures 25
through 29 show the dendrites in these voids and clearly
illustrate that all are of the same type. This defect shall be
referred to as a "collar defect", since it appears in the collar
area of the welds. Collar defects were found in welds TW-1, TW-
2, TW-3, TW-4 and TW-5.

Metallography

Typical microstructures of thermite welds are shown in
Figures 30 through 35. All thermite weld microstructures
observed were nearly fully pearlitic with a small amount of
proeutectoid ferrite in the prior austenite grain boundaries and
around inclusions. The inclusions in the weld metal were
spherical. The inclusion volume fraction measurements of the
thermite welds are shown in Table V. The lowest value obtained
for thermite weld inclusion volume fraction percentage was .11
+/- .03 (%), while the highest was .21 +/- .07 (%). When the 95%
confidence limits are applied to all of the data, a ranking of
the specimens on the basis of inclusion levels could not be made.

The ferrite volume fractions of the thermite welds are found in Table VI. There was also much scatter in these data, with the lowest value measured at .09 +/- .07 (%) and the highest at 1.56 +/- .26 (%).

Chemical Analysis

Results of chemical analysis are shown in Table VII. The percent carbon of the thermite welds ranged from .52 to .76 and the percent manganese ranged from .84 to 1.60.

ELECTROSLAG WELDS

Impact Testing

The CVN dial energies for electroslag weld specimens are shown in Table VIII. Dial energies ranged from 1.5 to 3.5 ft-lb. Scanning electron microscopy of the broken specimens revealed brittle cleavage fracture with a small amount of ductile dimple fracture along grain boundaries, as shown in Figures 36 to 39. Some possible fracture initiation sites were found at inclusions, as seen in Figure 40. Energy Dispersive X-Ray analysis was used to determine the composition of these inclusions. Traces of copper, aluminum, and silicon were found, but manganese and sulphur yielded strong peaks relative to the others, Figure 41. It was concluded that at least some of the inclusions were

manganese sulphide, and that other elements showing smaller peaks were either trace elements in the metal or oxide inclusions.

Tensile Testing

The results of the tensile tests of electroslag weld metal specimens are shown in Table IX. The electroslag welds exhibited an average ultimate tensile strength of 126 +/- 5 ksi (865 MPa) and an average .2% offset yield strength of 81 ksi +/- 11.6 (554 MPa). The failure surfaces of the electroslag tensile bars resembled the fracture surfaces of the Charpy impact specimens; with primarily brittle cleavage and a small amount of ductile dimple fracture as can be seen in the SEM micrographs, Figures 42 through 45.

Metallography

Typical microstructures of electroslag welds are shown in Figures 46 through 53. Tables X and XI give the inclusion and ferrite volume fractions, respectively, for the electroslag rail weld metal. The inclusion volume fraction percentages ranged from .10 +/- .03 to .17 +/- .05, and the ferrite volume fractions ranged from .02 +/- .02 to .55 +/- .78 (%). As in the case of the thermite welds, no ranking could be determined.

Wear and RCF Tests

The hardnesses of the tested rollers are listed in Table XII. The plots of weight loss versus revolutions showed a linear relationship with a run-in period of approximately 100 revolutions at contact pressures of 1220 N/sq.mm, and 200 to 400 cycles for the lower loads. A typical plot is shown in Figure 54. One test was scheduled to be run at the 500 N/sq.mm pressure, but it was not possible to maintain Type III (the most severe and reproducible type of metal-on-metal wear) at that pressure. The pressure was increased to 700 and then to 900 N/sq.mm before the rollers maintained Type III wear conditions. Type III wear is found on railroad rails and is shown in Figure 55 on a test roller surface. The results of the wear tests are collected in Table XIII. Wear rates were calculated using the linear portions of the weight loss vs. revolutions curves. Figure 56 shows the relationship between hardness and wear rate for a contact pressure of 1220 N/sq.mm. The data were combined with rail steel data from another study [36] to plot the graphs of wear rate versus hardness for contact pressures of 1220 and 900 N/sq.mm, respectively, shown in Figures 57 and 58. In general the wear rate increased with increasing contact pressure and decreasing hardness.

The RCF test results are shown in Table XIV. Gross failure, typified by angular cracks in the rolling direction, and spalling, is shown in Figure 59. The results are plotted as life

against hardness, Figure 60, for a contact pressure of 1302 N/sq.mm. These data were combined with data from a rail steel study [37] for comparison. The resulting plot for a contact pressure of 1302 N/sq.mm is shown in Figure 61. In general, the RCF sample life decreases with increasing contact pressure, and increases with increasing hardness.

Heat-Affected Zones

The heat-affected zones of the eight electroslag welds are shown from a top view in Figures 62 through 69. All of the HAZ's were similar and considered normal.

<u>DISCUSSION</u>

THERMITE WELD EXAMINATION

Two thermite welds judged defective by the ultrasonic test car did contain small "collar defects" (welds TW-1 and TW-2). The three welds judged to be acceptable (welds TW-3, TW-4, and TW-5) also exhibited the same defect. In the case of rejected weld TW-2, only the collar defect (Figures 22 and 23) was found. Thermite weld TW-1 also contained other small defects. Analysis of the situation raises the important question of why weld TW-2 was judged defective while welds TW-3, TW-4, and TW-5 were not. This in turn raises several questions regarding the detection ability of the ultrasonic test method employed, and further about reliability of thermite rail welds.

In the Introduction, statistics were quoted which stated that thermite welds failed up to 100 times more often than factory-made rail welds. The results of the current study show that it is possible for an otherwise perfect weld with a collar defect to either pass (as in the case of welds TW-3, TW-4, TW-5) or fail (as in the case of weld TW-2) ultrasonic inspection. The first question that arises from these findings is could the defect be seen by the ultrasonic detector? It is considered unlikely that the Sperry Rail Car can detect a defect this far from the center of

the weld. If the detector were to run along the top of the rail and reach the critical foot area, the area scanned would be as shown in Figure 70. It appears that the collar defect is well out of that range. The proprietary Sperry detection system probably scans this area using detectors, and scans the head area using a magnetic induction technique. The minimum size of a defect that can be detected is ten percent of the head cross-sectional area [38]. The geometry of the rail makes ultrasonic inspection difficult, and reaching the collar area nearly impossible.

The collar defect itself consists of a cluster of spherical voids with dendrites in evidence. It appears in the same position in all of the welds, with the exception of the very porous weld TW-6. The voids in the collar defect were determined by scanning electron microscopy to be shrinkage voids, Figures 25 through 29. The SEM micrographs in the figures show clusters of defects, i.e. small areas of shrinkage broken up by the solid metal. This type of defect can be contrasted with a hot crack, which is caused by movement of the weld when the metal is still "mushy" in consistency. Hot crack defects are usually in the form of a crack caused by planar movement, as their name suggests. It follows that the collar defect found common to all of the thermite welds is not related to hot cracking but that it originated during the welding process.

One explanation for the occurrence of the collar defect is that the fluidity and flow pattern of the metal at the critical position is not ideal for filling the mold pattern before

solidification takes place. Risers and sprues are designed to account for this. A thermite weld with proper risers and sprues can run short of fluid material if the rails are spaced too far apart, if the crucible is tapped too late and consequently there is not enough heat remaining to allow the metal to flow freely, or if preheat is insufficient and the molten steel cools too rapidly when it comes in contact with the colder rails. These situations could be avoided if the welding instructions were accurately followed. Possibly, the positions of the risers or timing of the automatic tapper, and therefore the fluidity of the steel, are not optimum for total filling of the mold. Analysis of the temperature and flow patterns in a casting with a shape as complicated as a thermite weld is an extremely difficult task. A simpler solution to the problem may be to experiment with different riser, sprue, and tapper combinations, with all other process procedures and conditions according to instructions. Chiseling or shearing in the defect area may also be effective, provided the defect is completely removed and there are no stray chisel marks which can initiate cracks. Shearing in the area where the shoulder defect is found has been performed. Weld TW-4 was sheared in this area demonstrating that some welders were trained to attempt to eliminate this defect. It is interesting to note that on that particular weld, the defect was not completely removed and was still detected by radiography.

However, before taking steps to eliminate the collar defect, it must first be shown to present a threat to the integrity of the

weld or that it is causing spurious ultrasonic results. Is the shoulder defect likely to initiate a failure? The fact that some welders have been trained to shear this location raises some suspicion. Obviously the instructions to shear the weld at that point was made by someone other than the welder, so there must have been some concern either by the welding company who trains the welders (or the railroad who trains the welders) or from the engineering department of the railroad. This cluster formation can be removed if the welder chisels deep enough. The Norfolk and Southern Railroad [39] has found that the collar defect seriously compromises weld integrity so they therefore require that it be removed from all thermite welds by grinding the weld flush with the rail.

The role of the collar defect in thermite weld failure data is unclear. While AREA was still keeping records of rail weld failures, two of the types of thermite welds used employed slightly different preheating methods. These types of thermite welding, brand-named Exomet and Thermex, pre-dated the Orgotherm, Boutet and Thermit methods in use today. The older methods heated the rails before welding in two ways: 1) an exothermic material was burned inside the shell molds, which were connected to the disposable crucible, and 2) an excess of molten material "preheated" the rail ends by washing over them into a pan placed below the weld area [8,40,41]. The differences in heating methods corresponded to differences in the mold configurations. Sprues and risers were placed in different locations than those used in the Boutet

process. This is especially true of side-pour methods. The Exomet and Thermex methods were later replaced by the Orgotherm and Boutet methods, which use the flame preheat. It is possible that the shoulder defect is a property of the newer thermite welds, since all of the welds used in this investigation were of the Boutet brand. The Orgotherm brand uses a process similar to Boutet. Data for all weld types are given in the failure statistics quoted previously; some of the data are for the older types of thermite welds. In none of the data detailing failure causes of thermite welds was a failure reported which initiated at the collar area by a shrinkage void [24,25,28,29]. Failures were reported for Orgotherm welds which initiated at the weld collar area from oxide on the surface [28]. The majority of failures in all thermite welds was the result of oxide inclusions in the rail head. Since no data on thermite weld failures since 1970 is publicly available, it is possible that the appearance of the collar defect has accompanied changes in welding practices and that the full effect of this defect is largely unknown.

In weld TW-1 the common collar defect as well as other small defects were found by radiography. This again raises the question of what the ultrasonic test car can indeed detect, and which defects would be cause for rejecting the weld. In England, British Rail uses a point system to determine whether a weld is accepted or rejected [42]. The system assigns a number of points to a defect depending on its size and location. The head and the center of the foot are high score areas, and the larger the defect, the more

points assigned to it. The rejection criterion is that the weld
not exceed a maximum number of points. Other countries also use
point systems. In the United States, some railroads use criteria
based on their own inspection of the welds. Others, including
Amtrak in this case, hire an ultrasonic testing service to inspect
the welds and pass or fail them according to their own system.

The thermite welds received for this study were not
accompanied by test records. Information relating to why the welds
were rejected would have been helpful in determining just what the
failure criteria for these welds, and for the railroad, are.

In weld TW-6 it is obvious that the welding procedure followed
was at fault. In the other five it is possible that everything was
carried out correctly, according to instructions. The inconsistent
data from this investigation show that it is possible for
essentially identical welds to be both rejected and passed by an
ultrasonic test.

The defect that was found to be common in the welds in this
study may or may not be the cause of spurious ultrasonic data.
More study is required to determine this. A way to test the
hypothesis that this defect is triggering random ultrasonic
indications would be to make a large number of welds, some sheared
in the collar area and some not. These welds would then be
ultrasonically tested in the same way as the welds used in this
investigation and then sectioned to see if erratic results are
obtained. Also, the welds could be left in service and a long-term
study done relating the reliability of the welds to the presence of

the defect. The effect of shearing the defect area could also be examined in this way. It may also be possible to eliminate the defect altogether by changing the casting parameters, instead of running expensive long-term experiments in an effort to determine if the shoulder defect is causing the spurious ultrasonic data.

THERMITE VS. ELECTROSLAG COMPARISON

Metallography

Inclusion volume fractions were measured for thermite welds, electroslag welds, and rail steel. The volume fractions of inclusions found in Tables V and X may be compared with those of a similar study by Schroeder and Poirier [9,16,18] found in Table XV. They used sections from the center of the weld, about 2.5 cm below the running surface and parallel to it. Their data were not found to depend on any weld variables [16]. Also included in Table XV are comparable head-hardened and standard rail inclusion volume fractions taken from samples transverse to the rail rolling direction; the shapes observed were round and smooth giving the most reliable data possible.

It can be assumed that the data for the rail steel and for the thermite welds in this study were comparable and consistent, since precautions were taken to ensure consistency of in-house data. The Schroeder and Poirier data were generated using a quantitative image analyzer, which determines the size and dispersion of a

constituent by sorting the pixels on a computer screen by intensity or color within a given size range. In the Schroeder and Poirier work and in this investigation the same 400 sq.um upper limit on the size was used. It can be difficult to determine the difference, on the computer screen, between porosity and inclusions if they are the same intensity on the screen. This difficulty is also present with the microscope so care must be taken when using both methods. In this investigation when there was any doubt as to whether or not the object being counted was in fact an inclusion, the suspect image was observed using a differential interference contrast filter, with which the Nikon Epiphot is equipped. No details are given in the referenced work on how this differentiation was made using the image analyzer.

In both thermite weld studies, fields with indications measuring more than 400 sq.um were rejected. To determine the validity of rejecting these relatively large indications a point count was done in the present work at the same grid size and magnifications, but only indications covering more than nine grid points (400 sq.um) were counted. The count yielded a volume fraction of zero percent. It was concluded that the presence of large inclusions did not affect the results of the volume fraction estimates.

Much scatter was found in the inclusion volume fractions. When 95% confidence bands given in the Tables are applied, it is seen that there is no statistically significant difference between the inclusion levels measured in the six Amtrak thermite welds of

this investigation, Schroeder and Poiriers' thermite welds, rail steel, or the eight electroslag welds.

Ferrite volume fractions were measured for the thermite welds and for the electroslag welds, Tables VI and XI. The scatter in the ferrite measurements was even greater than for the inclusion volume fraction measurements. This is because the ferrite is not evenly dispersed, as the inclusions tend to be. This scatter makes quantitative comparison of the welds impossible, but it should be noted that some ferrite was found in all of the welds.

Hardness

Table XV contains hardness measurements of thermite welds from Schroeder and Poirier [18], taken in the weld zone. These are average values, each average unique for one weld. They are comparable to the thermite weld hardness levels and the electroslag weld metal hardnesses, found in Tables XVI and XVII, respectively.

The electroslag weld metal varies from the same hardness as the rail to about four points harder than the parent metal. The hardnesses of the weld metal range from 25 HRc to 31 HRc. The hardness varies with position in the weld, the web section having harder material. These welds were all made under the same conditions by the same people with the same materials. The hardness variation along the vertical axis in the electroslag welds could be due to chemistry differences. A chemistry gradient in this direction for electroslag welds has been documented [14].

Impact Properties

The Standard-size CVN dial energies reported in Table VIII are very similar to the data reported for both rail steel and thermite welds. Charpy key-hole specimens have been tested at temperatures as high as 212°F. The highest impact energy recorded was 10 ft-lb at that temperature [43]. Considering the scatter in the electroslag data and the thermite weld data, no conclusions can be drawn as to which one has the higher Charpy energy. They are both relatively brittle types of welds. This is not surprising since standard carbon rail steel itself has a low impact resistance of two to four ft-lbs. at room temperature, and both types of welds have larger grains than the parent metal.

ELECTROSLAG RAIL WELD INVESTIGATION

Experimental

This study made use of a small number of electroslag welds. When studying any type of welding, the number of welds must be large enough for the characteristics of the welding method to be determined. As the number of variables increases, so must the number of specimens. Ideally, each weld should have all of the types of samples removed from it for the sake of consistency. If this is not possible and the samples must be removed from different welds, a greater number of welds is needed to account for differences between them.

The size of the Amsler rollers and other test samples in relation to the size and odd shape of the rail weld limits the number of samples that may be taken from each weld. In this investigation it was found that the welds, even though they were made under the most controlled conditions possible, varied. Welds differed in the number of inclusions and amount of proeutectoid ferrite, and hardness. The variation was found to be less for Charpy impact toughness and tensile properties.

Another challenge faced in the study was extracting Amsler rollers from heat-affected zones. This is a good example of working with machining limitations imposed on a materials study. The rail sections were turned to an over-sized round stock and sent to a shop with a computer numerically controlled lathe for finishing, since the part is rather complex. The rollers were formed and removed one at a time from the bar with a parting tool. The etched heat-affected zone pattern shows up as a wavy darker region encircling the bar. It would be difficult to remove a sample wholly within the HAZ because of this irregularity of shape. It would also waste material and decrease the number of samples available for testing. Other studies have shown that even within the HAZ there is variation in grain size [14]. The zones were too narrow for any effect to be investigated using standard Amsler wear samples. It was hypothesized that the largest factor in predicting wear rate and RCF life would be the hardness of the material. By taking three samples, one definitely in the weld zone, one definitely in the heat-affected zone, and one perhaps in between,

trends with hardness were examined.

Rolling Contact Properties

Rails and rail welds can be characterized by their resistance to wear and fatigue resulting from rolling contact. The Amsler Twin Disk Testing Machine, Figure 18, simulates the types of damage seen in service in a representative and repeatable manner. The applicability of the Amsler tests to the study of rolling contact fatigue has been shown [33,34]. The twin disk machine was used in this investigation for testing dry sliding wear and rolling contact fatigue resistance of the ESRW weld metal and heat-affected zones. RCF is defined as surface-initiated failure characterized by a layer of plastic deformation with cracks running at an angle of 20 to 30 degrees to the surface in the rolling direction [34]. Macroscopically, pits can be seen on the surface, along with small cracks across the rolling surface.

The relationship between contact pressures and wear and rolling contact fatigue (RCF) resistance is of increasing interest to the railroad industry because of the desire to move to heavier axle loads. One goal in this part of the investigation was to establish a database for the RCF and wear behavior of ESRW weld and HAZ metal. The data presented here adds to the data already generated for rail steels. Recent studies [36,37] on rail steel have shown that wear rate and rolling contact fatigue resistance depend on hardness, which is directly related to the pearlite spacing. Wear rate increases with contact pressure, while RCF life

decreases. Small chemistry variations were not found to have an effect on the wear rate or on the RCF life.

Figure 56 shows that the wear rate of ESRW weld metal and HAZ show increasing wear resistance with increasing hardness at a contact pressure of 1220 N/sq.mm. Figures 57 and 58 show wear rate versus hardness plots for contact pressures of 1220 and 900 N/sq.mm, respectively, with the data from this study plotted with data from a previous investigation using heat-treated rail steel. The data points from the present work fit neatly into the scatter ranges of the previous data. The weld metal head section samples of hardness HRc 25 show very good repeatability. There is a possibility that the specimens from this study had slightly lower wear rates at the higher contact pressure, however, this cannot be stated conclusively from the graphs.

Figure 59 shows the relationship between rolling contact fatigue life and hardness for the electroslag weld metal and heat-affected zone at a contact pressure of 1302 N/sq.mm. The RCF life increases with hardness. The rolling contact fatigue plot in Figure 61 shows the relationship between hardness and RCF life for data from this study and those [37] of heat-treated rail steel of various hardnesses. All of the points lie within the same scatter band which shows increasing rolling contact fatigue life with increasing hardness.

CONCLUSIONS

Thermite Weld Failure Investigation

The collar defect was found in five otherwise sound welds, chosen at random. It is likely that most thermite welds made in the United States contain collar defects. Little information on the collar defect is available, yet it has been found by at least one major railroad, Norfolk and Southern, to be a serious potential cause of weld failures. The position of the collar defect, combined with the complicated shape of the weld, make inspection and monitoring of the defect difficult.

Electroslag Rail Weld Investigation

Electroslag weld metal was found to fracture in the same brittle manner as that of thermite welds and showed an average ultimate tensile strength of 126 ksi and .2% offset yield strength of 81 ksi. Standard room temperature Charpy V-Notch dial energies averaged 2.5 ft-lb.

Wear resistance and rolling contact fatigue life increased with increasing hardness and the data were consistent with that for standard carbon rail steel.

Thermite Weld vs. Electroslag Weld Comparison

Electroslag rail welds were found to be comparable to thermite rail welds in terms of inclusion and ferrite volume fraction, impact and tensile strength.

Electroslag rail welds appear to be as good as thermite welds in terms of mechanical properties, and at least as good as standard carbon rail steel in wear and RCF resistance. The electroslag welding method used has potential for use as an alternative field welding method.

RECOMMENDATIONS AND FUTURE WORK

The effect of the thermite weld collar defect on weld reliability needs to be documented so that railroads may be made aware of it.

Wear and RCF data for thermite welds is needed for comparing these properties to those of newer field welding methods.

Large-scale field trials of electroslag rails welds are needed so that the viability of the method can be fully evaluated.

REFERENCES

1. Knupp, G.G., et. al., "A Review of the Manufacture, Processing, and Use of Rail Steels in North America--A Report of AISI Technical Subcommittee on Rails and Accessories", ASTM Special Technical Publication 644, ASTM, Philadelphia, 1978, p.9.

2. Holbrook, Stewart H., The Story of American Railroads, Crown Publishing, New York, 1947, p.39.

3. McGannon, ed., The Making,Shaping and Treating of Steel, 9th edition, U.S. Steel, 1971, p.754.

4. Hauser, Daniel. Methods for Joining Rails: Survey Report. U.S. DOT-FRA July 1977.

5. American Railway Engineering Association Bulletin, volume 64, p.46.

6. Fricke, Hans D., "Thermit Welding", Metals Handbook, vol. 6, pp.692-704.

7. Key, A.J. "Thermit Welding". Thermite Welding Ltd. Great Britain.

8. "Continuous Welded Rail--Thermite Welding" AREA Bulletin, volume 68, Bulletin 605, 1967, p.398.

9. Schroeder, L.C. and Poirier, D.R. "Structure and Properties of Thermite Welds on Premium Rails". National Technical Information Service. Springfield, VA. December 1985.

10. Ashton, M.E., "Thermit Welding of Rails Steels", Railway Engineer, vol. 2, no. 3, May-June 1977, pp.40-45.

11. AMTRAK Joint Elimination Procedure. Amtrak, December 1984.

12. Hauser, Daniel. Methods for Joining Rails: Survey Report. U.S. DOT-FRA July 1977, p77.

13. "Electroslag Welding", Metals Handbook, volume 6, American Society for Metals (ASM), Metals Park, OH, 1986.

14. Scholl, M., Masters Thesis, Oregon Graduate Center, Beaverton, OR, 1981.

15. Schroeder, L. "Physical Metallurgy and Process Improvement of Thermite Rail Welds". University Microfilms. Ann Arbor, MI. 1982.

16. Schroeder, L.C. and Poirier, D.R. "The Mechanical Properties of Thermite Welds in Premium Alloy Rails". Materials Science and Engineering. Vol 63. pp 1-21. 1984.

17. Schroeder, L.C. and Poirier, D.R. "Thermite Rail Welds; The Process, Mechanical and Metallurgical Properties, and Possible Improvements", Railroad Rail Welding, Railway Systems and Management Association, Northfield, NJ, 1985.

18. Schroeder, L.C. and Poirier, D.R. "Structure and Properties of Thermite Welds in Rails". Research and Development. August 1982.

19. Jones, H.N. "Some Practical Considerations on the use of Flash-Butt and Thermite Welds on Track". Railroad Rail Welding, Railway Systems and Management Association, Northfield, NJ, 1985.

20. Meyers, J., Geiger, G.H., and Poirier, D.R. "Structure and Properties of Thermite Welds in Rails". AWS Conference Proceedings. 1982.

21. American Railway Engineering Association Bulletin, volume 72, Bulletin 638.

22. Lugg, P.J., "British Rail Experience with Rail Welding" Heavy Haul Conference Proceedings, 1982, p.216.

23. American Railway Engineering Association Bulletin, volume 77, Bulletin 656.

24. American Railway Engineering Association Bulletin, volume 70, Bulletin 619, pp. 684-698.

25. American Railway Engineering Association Bulletin, volume 67, Bulletin 598, pp. 423-428.

26. American Railway Engineering Association Bulletin, volume 65, Bulletin 584, p. 611.

27. American Railway Engineering Association Bulletin, volume 67, Bulletin 598, pp. 423-428.

28. American Railway Engineering Association Bulletin, volume 70, Bulletin 619, pp.699-709.

29. American Railway Engineering Association Bulletin, volume 68, Bulletin 605, pp.383-396.

30. ASTM 562, "Determining Volume Fraction by Systematic Manual Point Count", ASTM Annual Book of Standards, volume 01.02, ASTM, Philadelphia, 1987, p.725.

31. Turpin, Robert, Masters Thesis, Oregon Graduate Center, Beaverton, OR, 1981.

32. Venkataraman,S., Turpin, R.B., Devletian, J.H., Scholl, M., and Wood, W.E., "Electroslag Welding of Rails", Railroad Rail Welding, Railway Systems and Management Association, Northfield, NJ, 1985.

33. Hill, D.N. and Clayton, P., "The Development of a Laboratory Rolling Contact Fatigue Testing Procedure", British Rail Research Report TMMF 32, 1982.

34. Clayton, P. and Hill, D.N., "Rolling Contact Fatigue of a Rail Steel", Wear 117, 1987, pp. 319-374.

35. Krause, Hans and Lehna, Heribert, "Investigations of Tribological Characteristics of Rolling/Sliding Friction Systems by Means of Systematic Wear Experiments Under Well Defined Conditions", Proceedings of the International Symposium on Contact Mechanics and Wear of Rail/Wheel Systems II, July 1986, pub. by Univ. of Waterloo Press, pp. 253-268.

36. Danks, D., Ph.D Thesis, Oregon Graduate Center, Beaverton, OR, 1989.

37. Vivek, A.D., Ph.D Thesis, Oregon Graduate Institute, Beaverton, OR, 1990.

38. Private Communication, Sperry Testing Service, February, 1988.

39. Private Communication, Norfolk and Southern Railroad, September 1989.

40. Kannowski, K.H., "Continuous Welded Rail--Field Welding--Thermite Welding", AREA Bulletin, Volume 71, Bulletin 626, 1970, pp.654-656.

41. American Railway Engineering Association Bulletin, Bulletin No. 614.

42. Farley, P.G., "Ultrasonic Testing of Aluminothermic Repair Welds, <u>Metals Construction</u>, 1980.

43. American Railway Engineering Association Bulletin, Bulletin 649, p. 81.

44. American Railway Engineering Association Bulletin, volume 74, Bulletin 641, p.338.

APPENDIX ONE

DETAIL OF AMTRAK THERMITE WELDING PROCEDURE [11]

1. Make sure crucible is free of cracks, preheat.

2. Prepare rail ends:

   Record rail temperature, support ends, check gap, clean with a wire brush

3. Set gap to 1-1/4 inches. A crown of 1/32" under the ends of an 18" straight edge, Figure 4.

4. Inspect molds for cracks and apply, sealing to the rails with refractory cement or paste.

5. Fill crucible with charge, taking care not to dislodge the self-tapping thimble. Swing out to the side of the mold.

6. Preheat rail ends with oxy-propane torch for a minimum of five minutes depending on the size of the section being welded, weather, preheating method and equipment. May be slightly longer as necessary. Never exceed seven minutes.

7. Move crucible over mold, ignite, and pour.

8. After the weld cools to 2000°F (no time given; in practice this is usually about five minutes), remove supporting wedges and finish grind with a profile grinder.

9. Inspect visually after cleaning sand off weld.

APPENDIX TWO

NOTES ON ELECTROSLAG WELDING PROCEDURE

1. The copper starting block, Figure 12, had a specially
shaped trough machined in it. The shape and size of this area,
which ultimately determines the size and shape of the weld
reinforcement under the rail base, was the result of numerous
trial welds in the initial development program [14,31,32]. The
trough was lined with a proprietary ceramic material obtained
from Wilbanks International in Hillsboro, Oregon. The ceramic
was coarse grained and fairly porous. The composition was such
that any melted material from it was compatible with the
electroslag bath. The purpose of the ceramic liner was to retard
heat during weld initiation. It was found that this initial
retardation of heat transfer enables heat to build rapidly at the
rail bases. After the weld progresses up the rail joint, heat is
extracted at a more desirable rate. In order to start the weld
on the ceramic, a formed steel plate was placed on the ceramic
inside the trough. The plate made electrical contact with each
rail base so current flow could be established.

2. The weld starting procedure is complex and is a direct result of the limitations of the power supplies used. The two parallel power supplies were rated at a total current capacity of 1500 amps. However, at weld initiation and while the electroslag bath is in the rail base, current flows of over 2500 amps were incurred. While the power supplies could handle this for short periods of time, long sustained current flows at this level would cause the power supplies to shutdown. Therefore, the guide tube and the starting procedure were developed and modified to work with this limitation. The starting procedure would be much more straight-forward and consistent if power supplies capable of a sustained current of 2500 to 3000 amps were available.

3. In a field welding situation, for which the electroslag rail welding process was ultimately developed, the weld run-out could be removed almost immediately at the end of the weld using a hot chisel or, ideally, a hydraulic nipper as is currently used on thermite welds.

Table I. Miles of CWR Laid Per Year [44]

```
pre-1955.......................<90/yr
1956.............................461
1957.............................550
1958.............................460
1959............................1071
1960............................1261
1961............................1021
1962............................1494
1963............................1858
1964............................2385
1965............................2356
1966............................2731
1967............................2584
1968............................3186
1969............................3604
1970............................6178
1971............................4109
1972............................4434
1973............................4767
1974............................4457
1975............................4291
1976............................5952
1977............................6458
```

66,389

Table II. Thermite Weld Information Received

Weld Number	Condition (year made)
TW-1	Sperry Defect (1985)
TW-2	Sperry Defect (1985)
TW-3	U.T. "good" (1986)
TW-4	U.T. "good" (1986)
TW-5	U.T. "good" (1987)
TW-6	visual defects and U.T. rejection (1987)

Table III.   Amsler Wear Test Matrix

Contact Pressure [N/sq.mm]

700	900	1080	1200
			3H1
			3H2
		3H3	
			6H1
			6H2
	6H3		
	7L		
			7H1
			7H2
			7H3
	8L		
	8L		
			8H1
8H2			
			8H3

Table IV. Amsler Rolling Contact Fatigue Test Matrix

Contact Pressure [N/sq.mm]

1412	1302	1223	1161	1094
				3L
				3H1
	3H2			
3H3				
6L				
	6L			
	6H1			
	6H2			
				6H3
	7H1			
			7H2	
	7H3			
	8H1			
		8H2		
	8H3			

Table V. Volume Fraction of Inclusions in Thermite Welds

Weld	Volume Fraction of Inclusions
TW-1 (head section)	.12 +/- .03
(foot section)	.18 +/- .05
TW-2 (head section)	.11 +/- .03
(foot section)	.21 +/- .07
TW-3 (head section)	.14 +/- .05
(foot section)	.19 +/- .04
TW-4 (head section)	.13 +/- .04
(foot section)	.17 +/- .05
TW-5 (head section)	.18 +/- .06
(foot section)	.11 +/- .04
TW-6 (head section)	.25 +/- .05
(foot section)	.23 +/- .07

Table VI. Ferrite Volume Fraction of Thermite Welds

Weld	Ferrite Vol. Fraction Percentage
TW-1 (head section)	.55 +/- .17
TW-1 (foot section)	.19 +/- .07
TW-2 (head section)	.69 +/- .23
TW-2 (foot section)	.21 +/- .11
TW-3 (head section)	.10 +/- .07
TW-3 (foot section)	.17 +/- .09
TW-4 (head section)	.15 +/- .09
TW-4 (foot section)	.09 +/- .07
TW-5 (head section)	1.56 +/- .26
TW-5 (foot section)	1.15 +/- .23
TW-6 (head section)	.39 +/- .15
TW-6 (foot section)	.94 +/- .34

Table VII. Weld Chemical Analyses

Weld no.:	%C	%Mn	%Si	%Cu	%Cr	%S	%P
TW-1	.524	1.317	.607	.255	.103	.039	.039
TW-2	.762	.917	.263	.324	.095	.013	.019
TW-3	.524	1.597	.617	.077	.151	.026	.029
TW-4	.528	1.385	.542	.099	.045	.020	.030
TW-5	.757	.844	.251	<.001	.008	.029	.017
TW-6	.528	1.158	.582	.140	.132	.582	.032
ES-1	.583	.689	.251	.253	.008	.013	.016
ES-2	.539	.854	.295	.253	.013	.013	.016
ES-3	.579	.795	.269	.143	.021	.012	.017
ES-4	.541	.829	.289	.137	.012	.013	.016
ES-5	.528	.786	.287	.142	.012	.013	.015
ES-6	.519	.855	.311	.144	.012	.012	.018
ES-7	.542	.748	.271	.127	.012	.012	.017
ES-8	.550	.774	.256	.148	.011	.012	.015

Table VIII. Standard Charpy Dial Energies for
Electroslag Rail Welds

Weld-Part	Dial Energy		
ES1-1	2.5		
ES1-2	2.5		
ES1-3	2.5		
ES1-4	2.5		
ES1-5	2.0		
ES1-6	2.25	mean=2.38	std. dev.=.21
ES2-1	2.75		
ES2-2	2.5		
ES2-3	2.5		
ES2-4	2.75		
ES2-5	2.5		
ES2-6	2.5	mean=2.58	std. dev.=.13
ES4-1	2.0		
ES4-2	1.5		
ES4-3	1.5		
ES4-4	2.0		
ES4-5	2.5		
ES4-6	2.0	mean=1.92	std. dev.=.38
ES5-1	3.0		
ES5-2			
ES5-3	2.5		
ES5-4	3.5		
ES5-5	2.5		
ES5-6	2.5	mean=2.75	std. dev.=.42
		MEAN=2.41	STD. DEV.=.43

Table IX. Electroslag Weld Tensile Test Results

.Weld-Part	UTS [ksi]	RA [%]
ES1-1	134	*
ES1-2	125	2.5
ES1-3	123	1.9
ES1-4	128	1.9
	mean=128	mean=2.1
ES2-1	132	3.1
ES2-2	131	2.5
ES2-3	129	3.7
ES2-4	130	3.1
	mean=131	mean=3.1
ES4-1	123	4.3
ES4-2	118	3.1
ES4-3	119	3.1
ES4-4	129	2.5
ES4-5	133	*
	mean=122	mean=3.3
ES5-1	129	0.6
ES5-2	122	4.3
ES5-3	126	3.7
ES5-4	137	1.9
ES5-5	123	3.1
ES5-6	122	2.5
	mean=127	mean=2.7
	MEAN=126	MEAN=2.8
	STD. DEV.=5.0	STD. DEV.=0.94

* denotes a bar that failed in the heat-affected zone; UTS values
  not included in mean.

Table X. Inclusion Volume Fractions of Electroslag Welds

Weld	Inclusion Vol. Fraction Percentage
ES-1	.15 +/- .03
ES-2	.17 +/- .05
ES-3	.13 +/- .03
ES-4	.11 +/- .03
ES-5	.11 +/- .04
ES-6	.10 +/- .03
ES-7	.11 +/- .04
ES-8	.15 +/- .04

Table XI. Ferrite Volume Fraction of Electroslag Welds

Weld No.:	Ferrite Vol. Fraction Percentage
ES-1	.13 +/- .10
ES-2	.40 +/- .27
ES-3	.12 +/- .09
ES-4	.35 +/- .27
ES-5	.29 +/- .29
ES-6	.55 +/- .78
ES-7	.66 +/- .47
ES-8	.02 +/- .02

Table XII. Hardnesses of Amsler Rollers (Average of 6 points)

WEAR SAMPLES			RCF SAMPLES	
Specimen	HRc--ave.		Specimen	HRc--ave.
3H2-1220	33		3L-1094	31
3H3-1080	28		3H1-1094	24
			3H2-1302	26
6H1-1220	25		3H3-1412	28
6H2-1220	28			
6H3-900	30		6L-1412	30
			6L-1302	29
7L-1220	29		6H1-1302	23
7L-900	28		6H2-1302	27
7H1-1220	25		6H3-1094	31
7H2-1220	28			
7H3-1220	33		7H1-1302	23
			7H2-1161	26
8L-900	30		7H3-1302	30
*8L-500	31			
8H1-1220	25		8H1-1302	24
8H2-700	27		8H2-1223	28
8H3-1220	32		8H3-1302	34

Notes:

Specimen codes represent weld number and location-contact pressure [N/sq.mm]

H's denote head section rollers; L's denote Web Section Rollers

* 8L-'500' showed Type III wear at 900 N/sq.mm, although the test was started at 500 N/sq.mm

Table XIII. Results of Amsler Wear Tests

Specimen Location	Contact Pressure [N/sq.mm]	Ave. Hardness [HRc]	Wear Rate [ug/m rolled]
7L	1220	29	102,234
8H1	1220	25	106,897
6H1	1220	25	101,317
7H3	1220	33	60,651
8H3	1220	32	93,719
7H1	1220	25	103,574
3H2	1220	33	78,693
6H2	1220	28	100,019
7H2	1220	28	138,502
3H3	1080	28	126,595
6H3	900	31	42,602
8L	900	30	21,683
7L	900	28	44,317
8H2	700	27	19,105
8L	900	31	28,303

*Specimen Location Code:
  Weld Number,   H = Head of Rail,   1 = Weld Metal
                 L = Web of Rail,   3 = HAZ
                                     2 = Combination

Table XIV. Results of Rolling Contact Fatigue Tests

Specimen Location*	Contact Pressure [N/sq.mm]	Ave. Hardness [HRc]	Cycles to Failure
7H3	1302	30	394,120
8H3	1302	34	412,760
6H2	1302	27	214,580
3H2	1302	26	208,940
6H1	1302	23	248,490
8H1	1302	24	223,490
7H1	1302	23	185,880
6L	1302	29	205,960
3H3	1412	28	67,200
6L	1412	30	160,540
3H1	1094	24	307,260
6H3	1094	31	649,190
8H2	1223	28	261,980
7H2	1161	26	282,560

*Specimen Location Code:

Weld Number,	H = Head of Rail,	1 = Weld Metal
	L = Web of Rail,	3 = HAZ
		2 = Combination

Table XV. Thermite Weld and Rail Steel Comparison Data

Source	HRc (Brinell)	Inclusion Vol.Fraction Percentage
Schroeder/ Poirier	(std. rail [18])	(premium rail [16,17])
	32(297)	.29 +/- .06
	30(283)	.44 +/- .08
	30(283)	.36 +/- .08
	33(305)	.24 +/- .06
		.28 +/- .07
		.49 +/- .09
ogc (unpublished)		.12 +/- .06
		.21 +/- .08

Table XVI. Thermite Weld Metal Hardnesses

Weld Number		HK	Brinell	HRc
TW-1	head	334	305	32
	foot	359	332	35
TW-2	head	329	300	32
	foot	332	303	32
TW-3	head	375	347	37
	foot	373	345	37
TW-4	head	345	316	33
	foot	347	318	34
TW-5	head	334	305	32
	foot	367	339	36
TW-6	head	319	291	31
	foot	330	301	32

Table XVII.   Electroslag Weld Metal Hardnesses

Weld Number	HRc	HB (by table conversion)
ES-1 head	27	265
web	32	297
ES-2 head	25	255
web	30	283
ES-3 head	24	250
web	30	283
ES-4 head	23	245
web	29	276
ES-5 head	23	245
web	31	290
ES-6 head	25	255
web	29	276
ES-7 head	23	245
web	29	276
ES-8 head	23	245
web	30	283
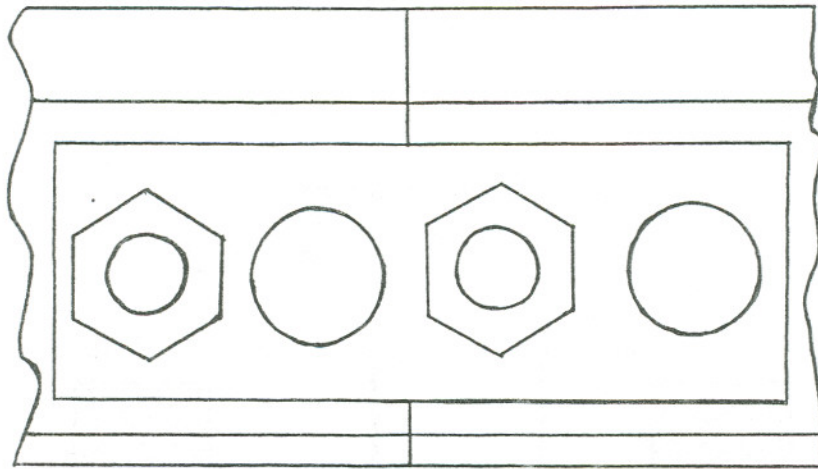
Longitudinal View
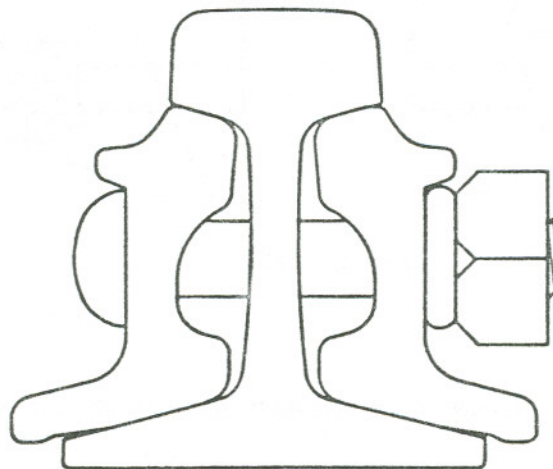
Transverse View

Figure 1. Bolted Rail Fishplate Connection

Force = 50-65 tons
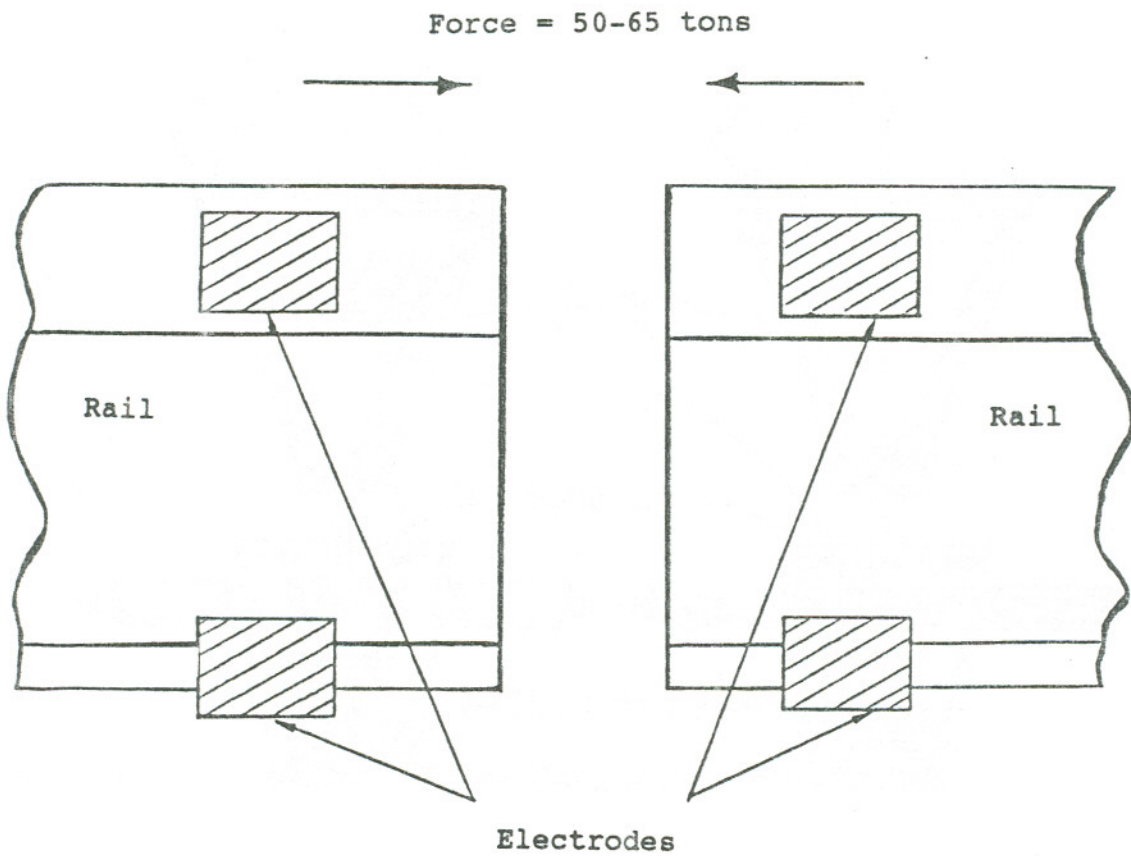
Figure 2. Electric Flash-Butt Welding Schematic
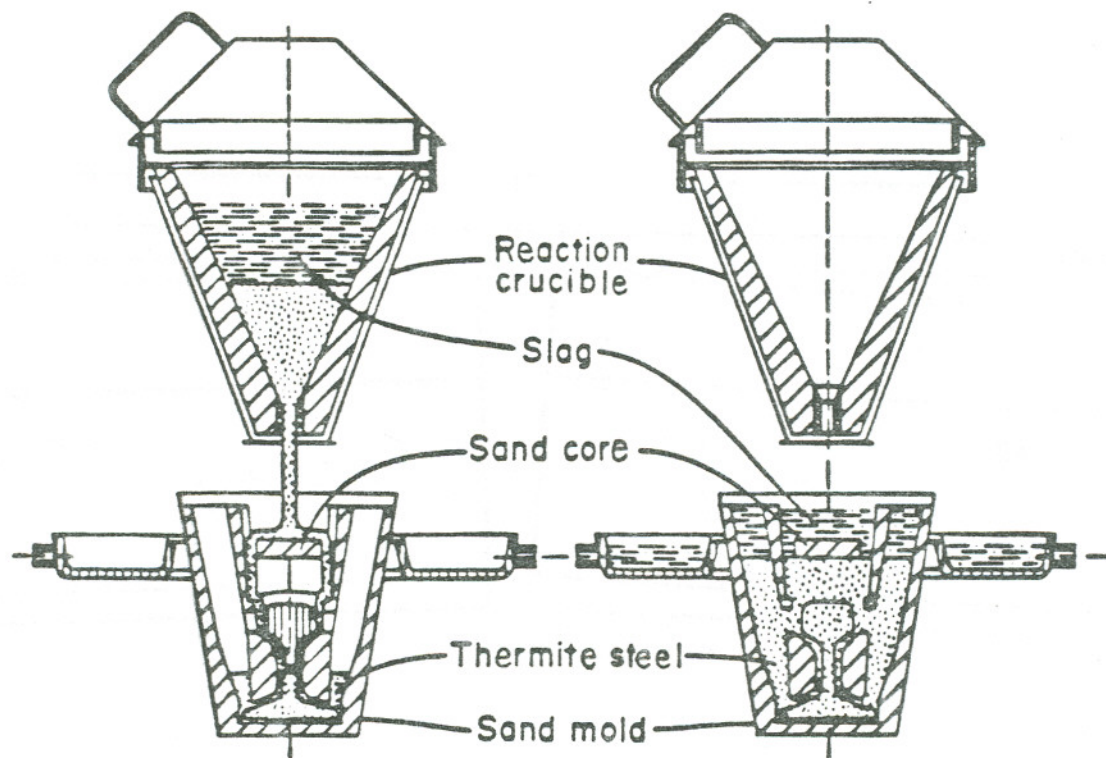
Figure 3. Thermite Rail Welding Schematic
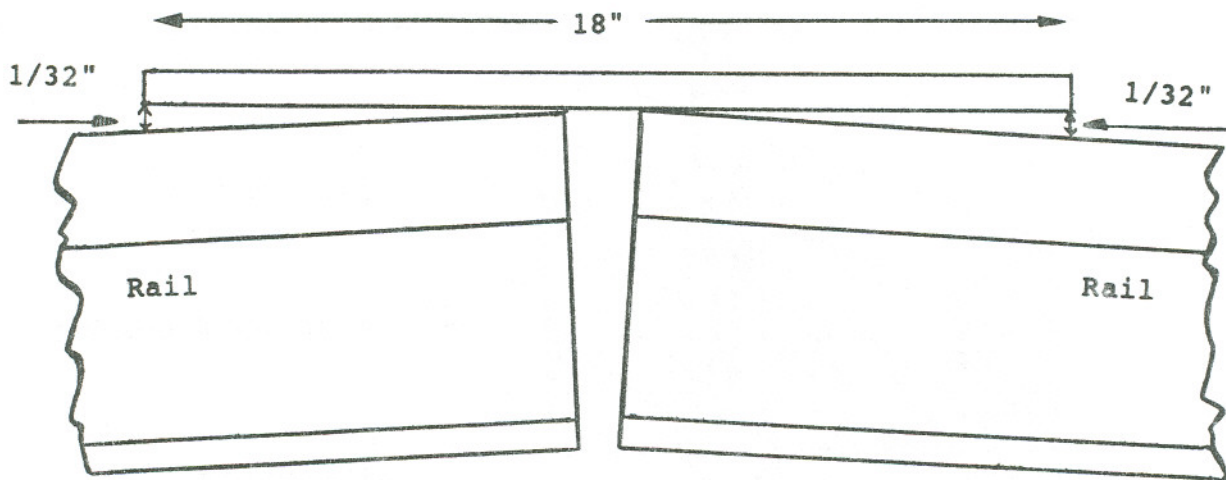
Figure 4. Rail Welding "Crown"
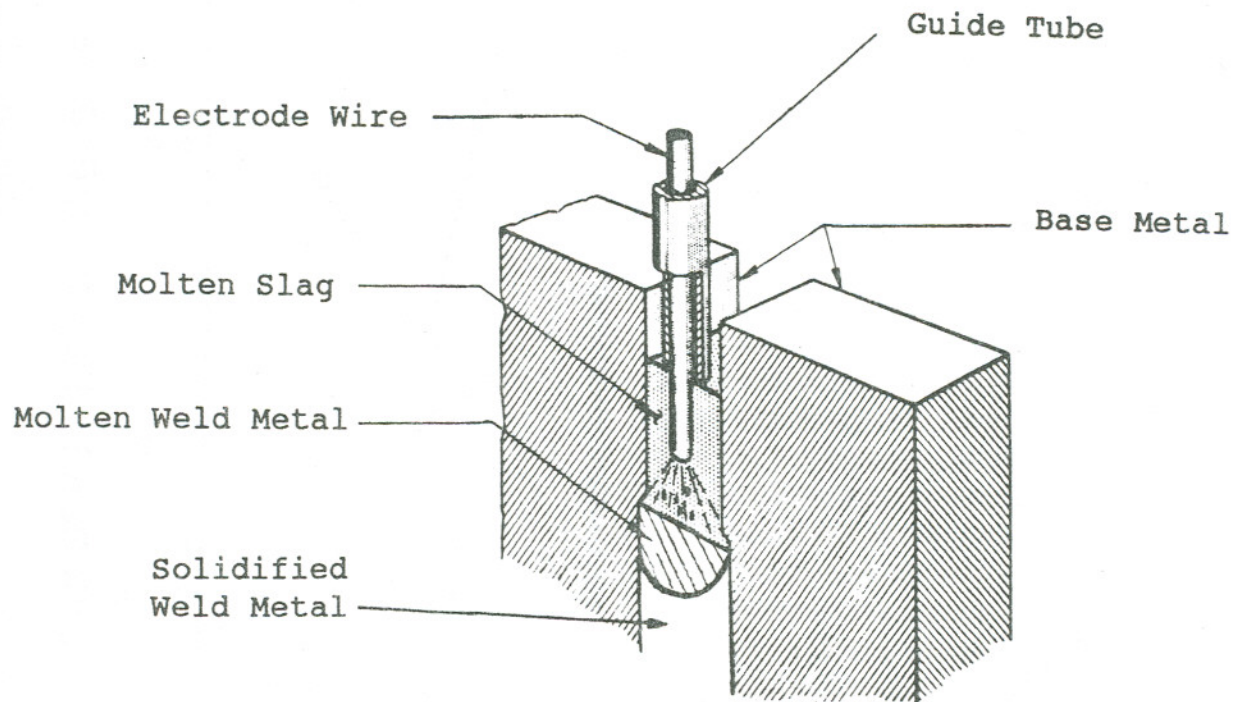
Figure 5. Electroslag Welding Schematic
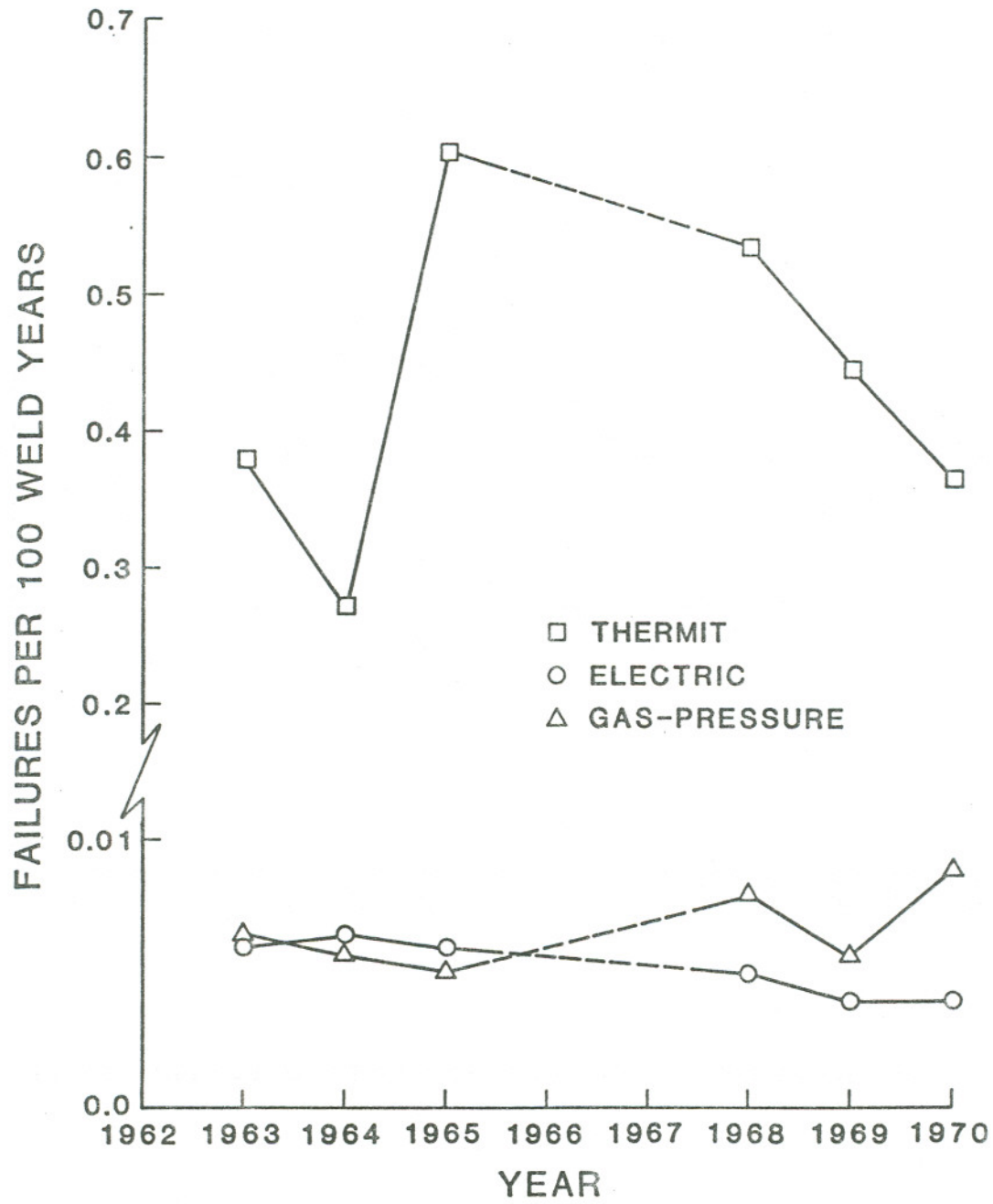
Figure 6. Rail Weld Failure Rates in Failures per 100 Weld-years
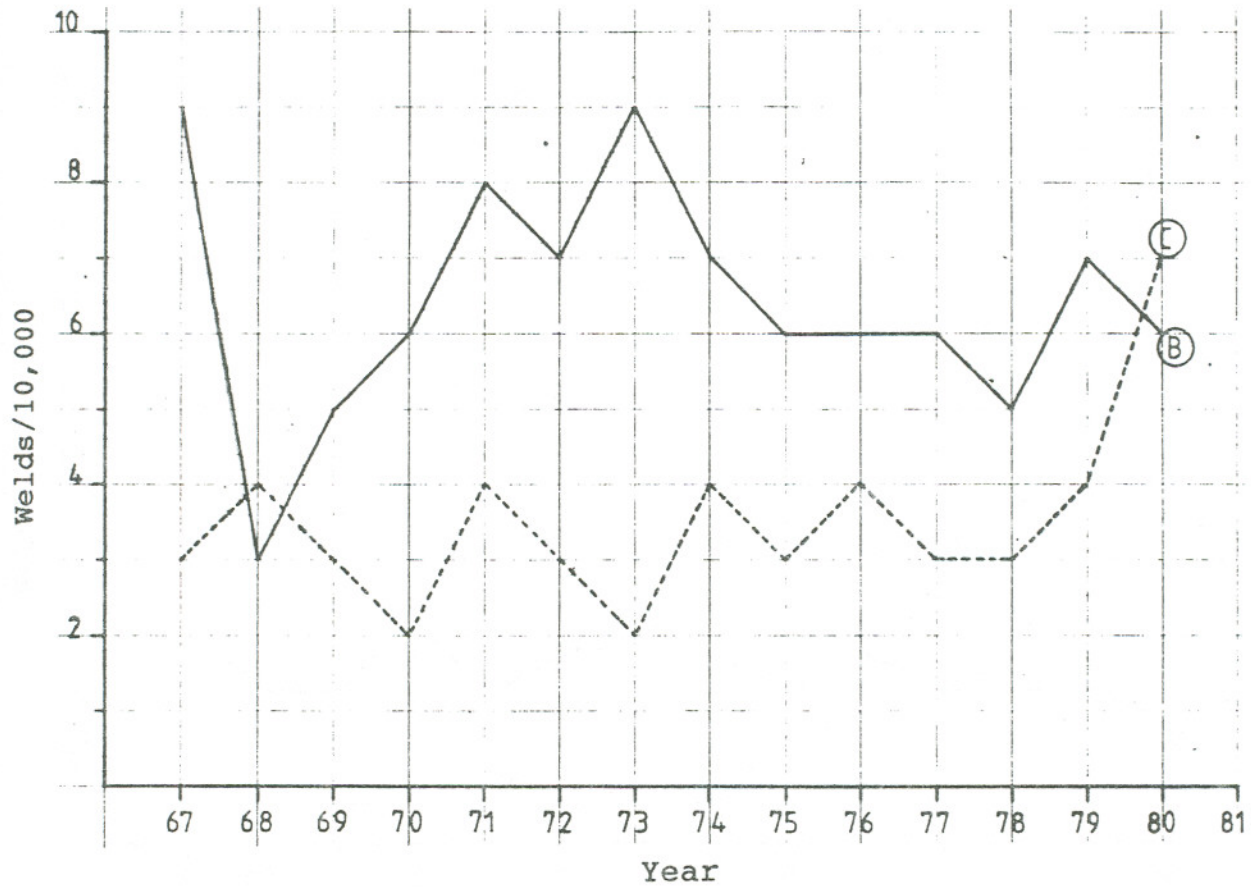
Broken and Cracked Thermite Welds per 10,000 Population

Figure 7a. British Rail Weld Failure Statistics
for Thermite Welds [22]
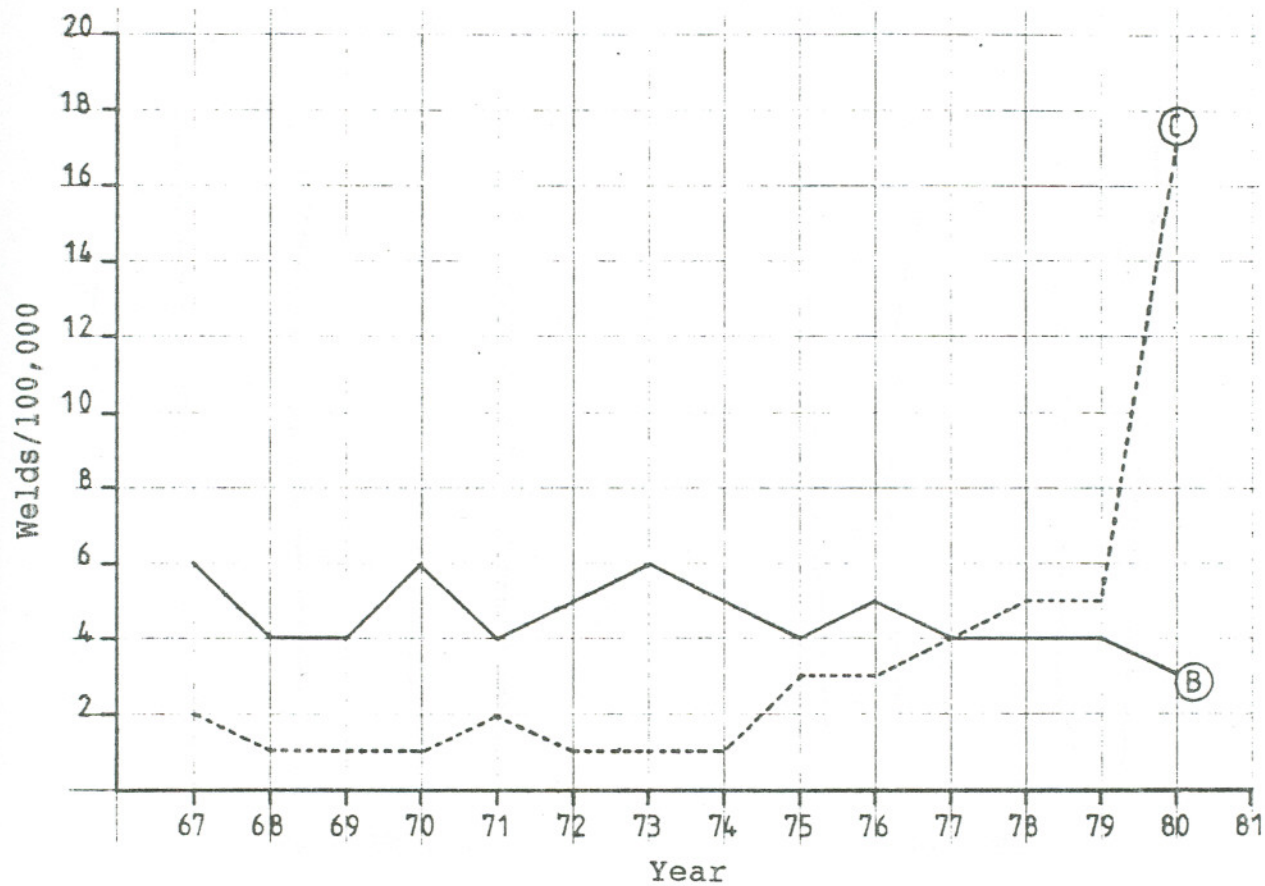
Broken and Cracked Flash Welds per 100,000 Population

Figure 7b. British Rail Weld Failure Statistics
for Flash Welds [22]

Weld TW-1   Weld TW-2
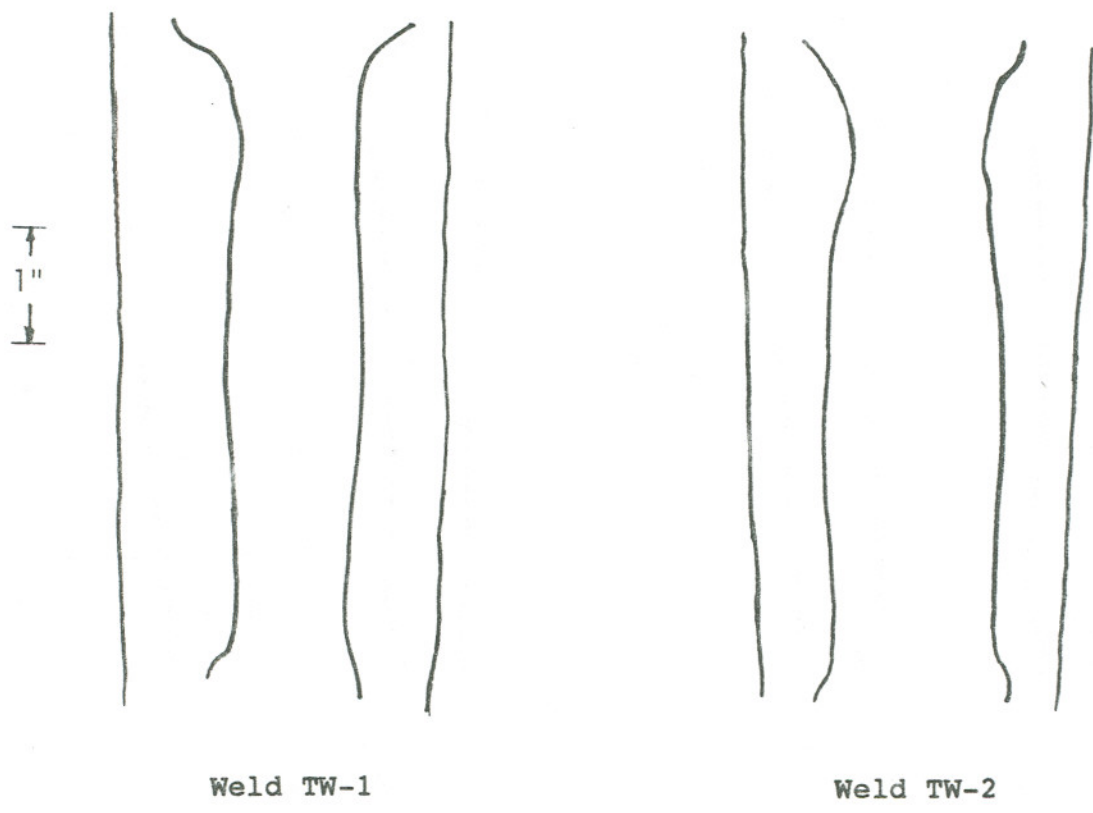
Figure 8a. Thermite Weld Heat-Affected Zone Traces
Welds TW-1 and TW-2

Weld TW-3   Weld TW-4
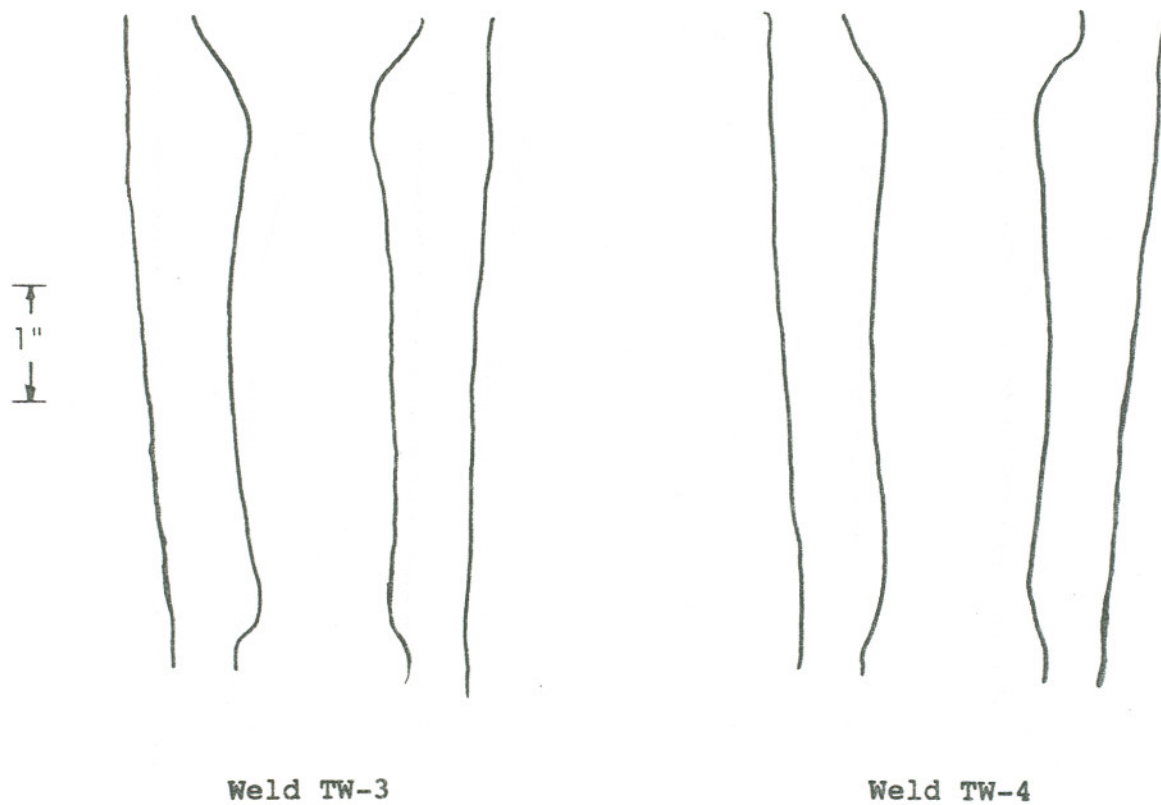
Figure 8b. Thermite Weld Heat-Affected Zone Traces
Welds TW-3 and TW-4

Weld TW-5   Weld TW-6
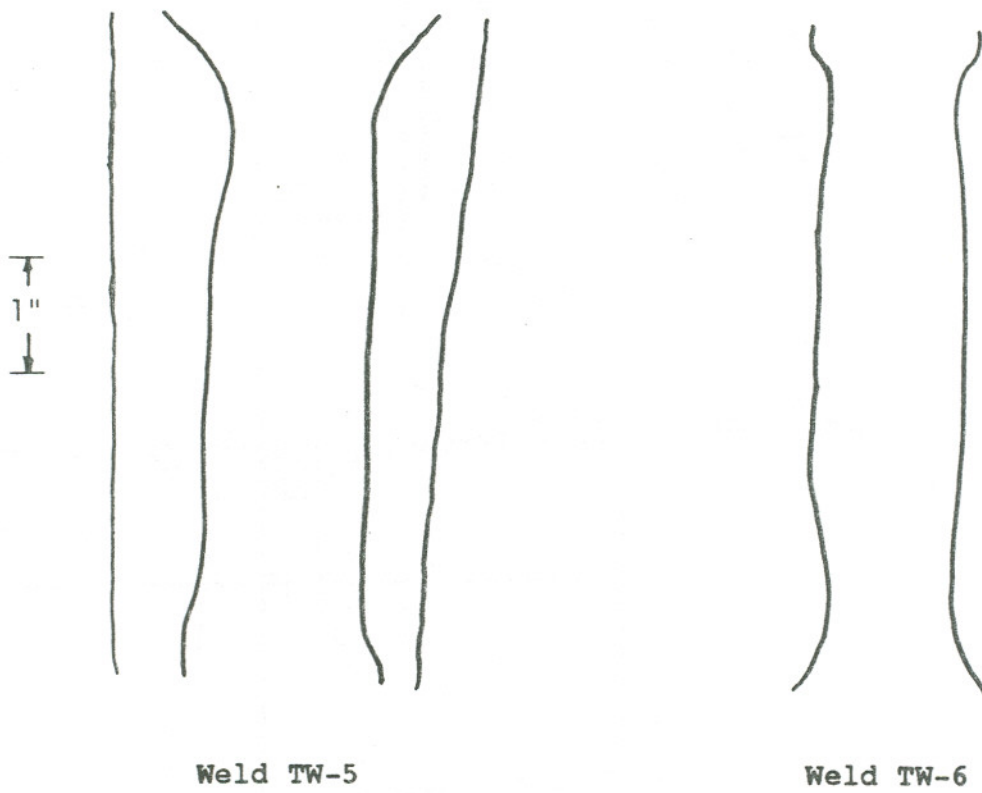
Figure 8c. Thermite Weld Heat-Affected Zone Traces
Welds TW-5 and TW-6

A-A:
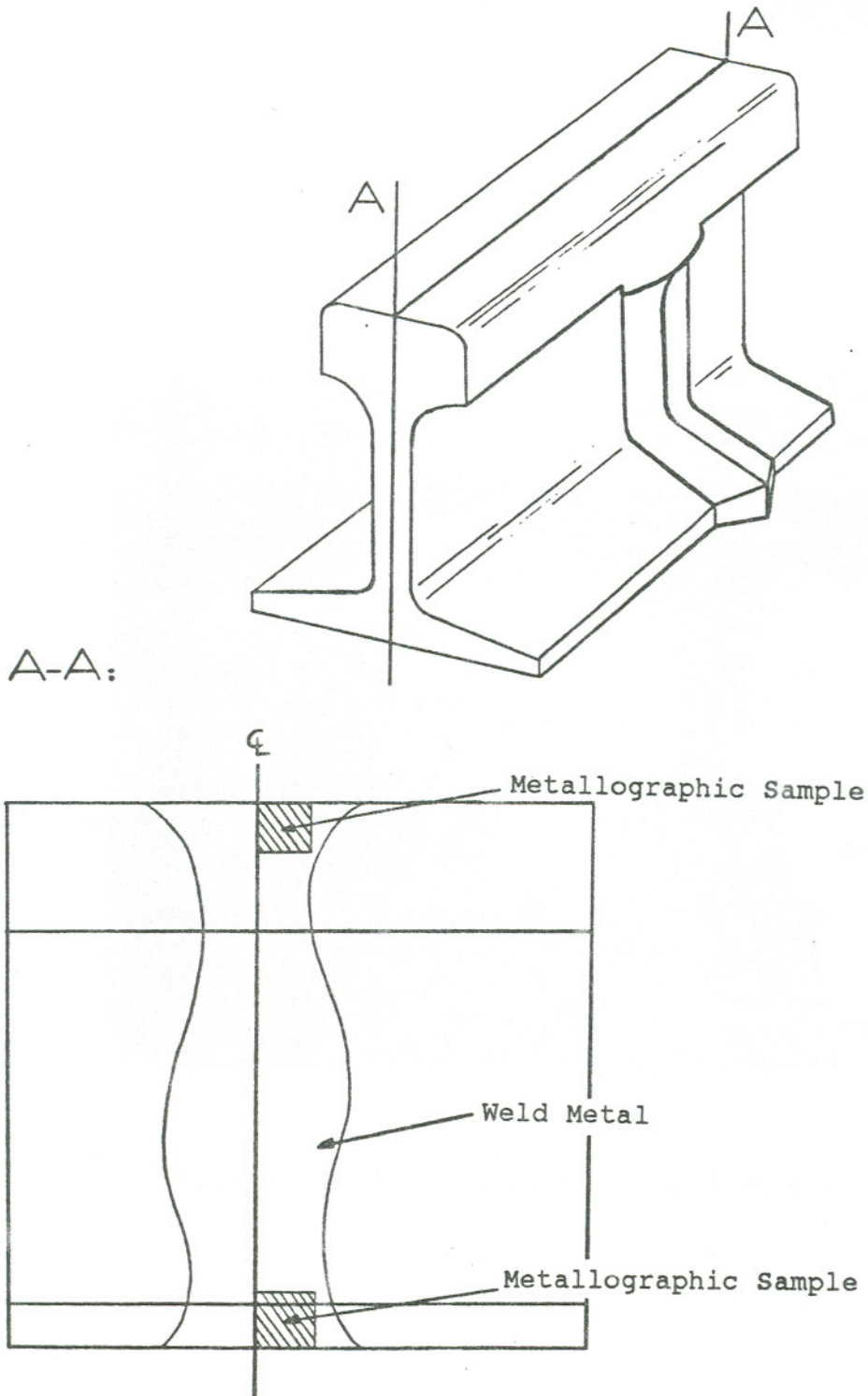
Figure 9. Thermite Weld Metallographic Sample Locations
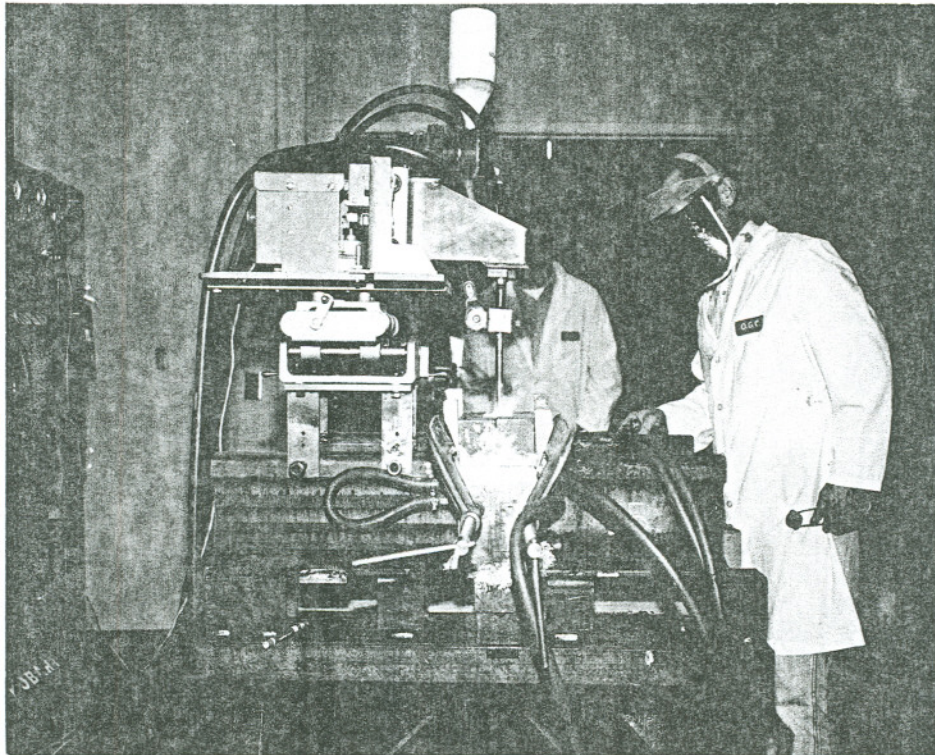
Figure 10. Electroslag Rail Welding Fixture

0.500 Steel Plate
10.0 Long

0.500 Tube
0.180 Wall

Alloy Plate starts
at this point when
rail head alloying
is required
(The last 41/2")
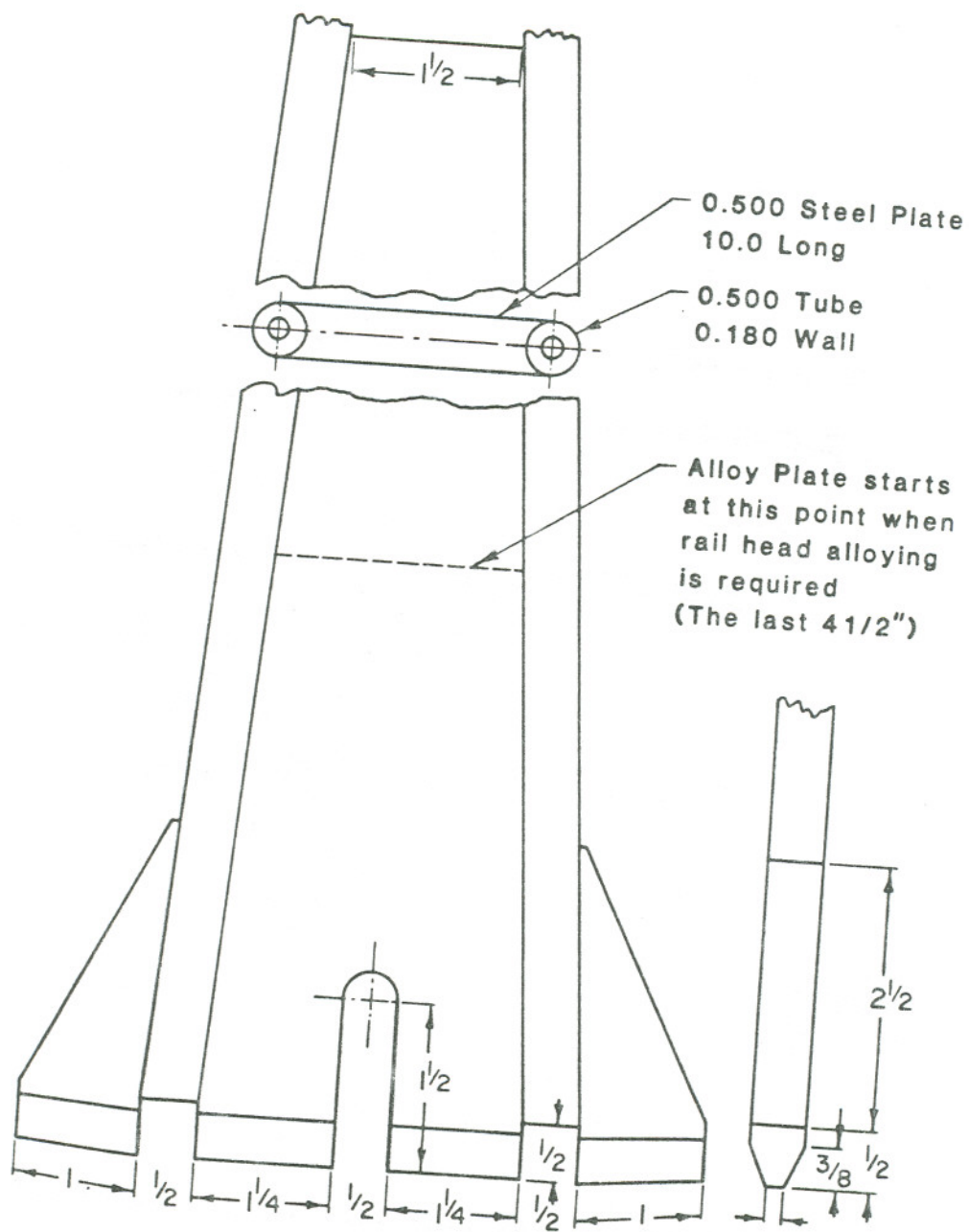
Figure 11. Electroslag Rail Welding Consumable Guide Tube
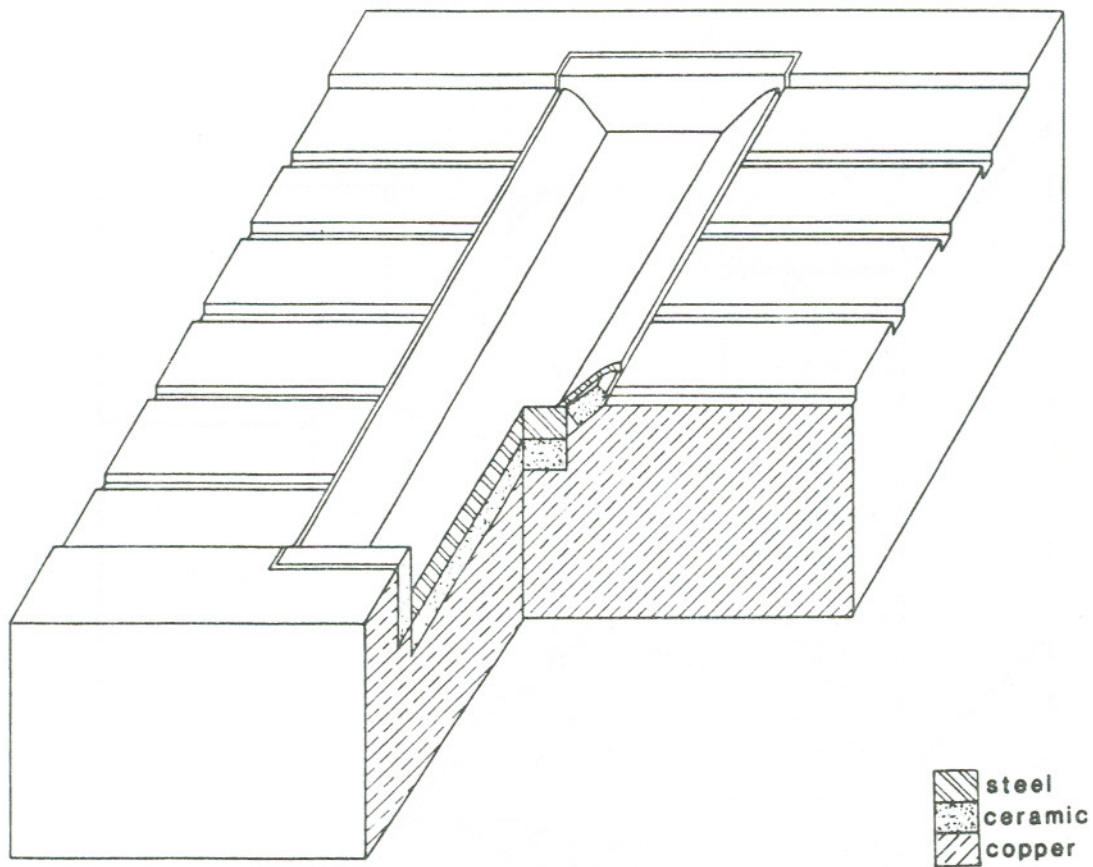
Figure 12. Electroslag Rail Welding Starting Block
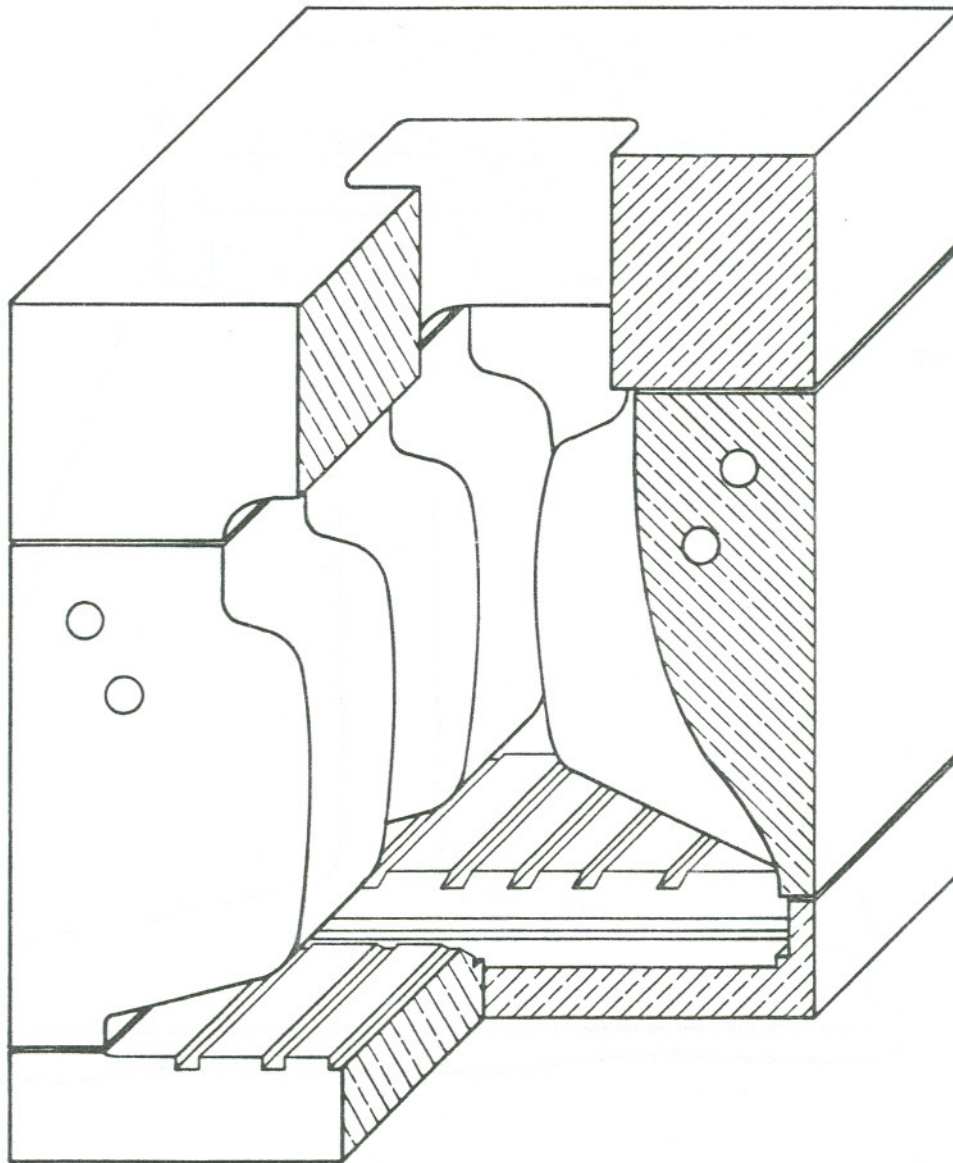
Figure 13. Electroslag Rail Welding Copper Cooling Shoes
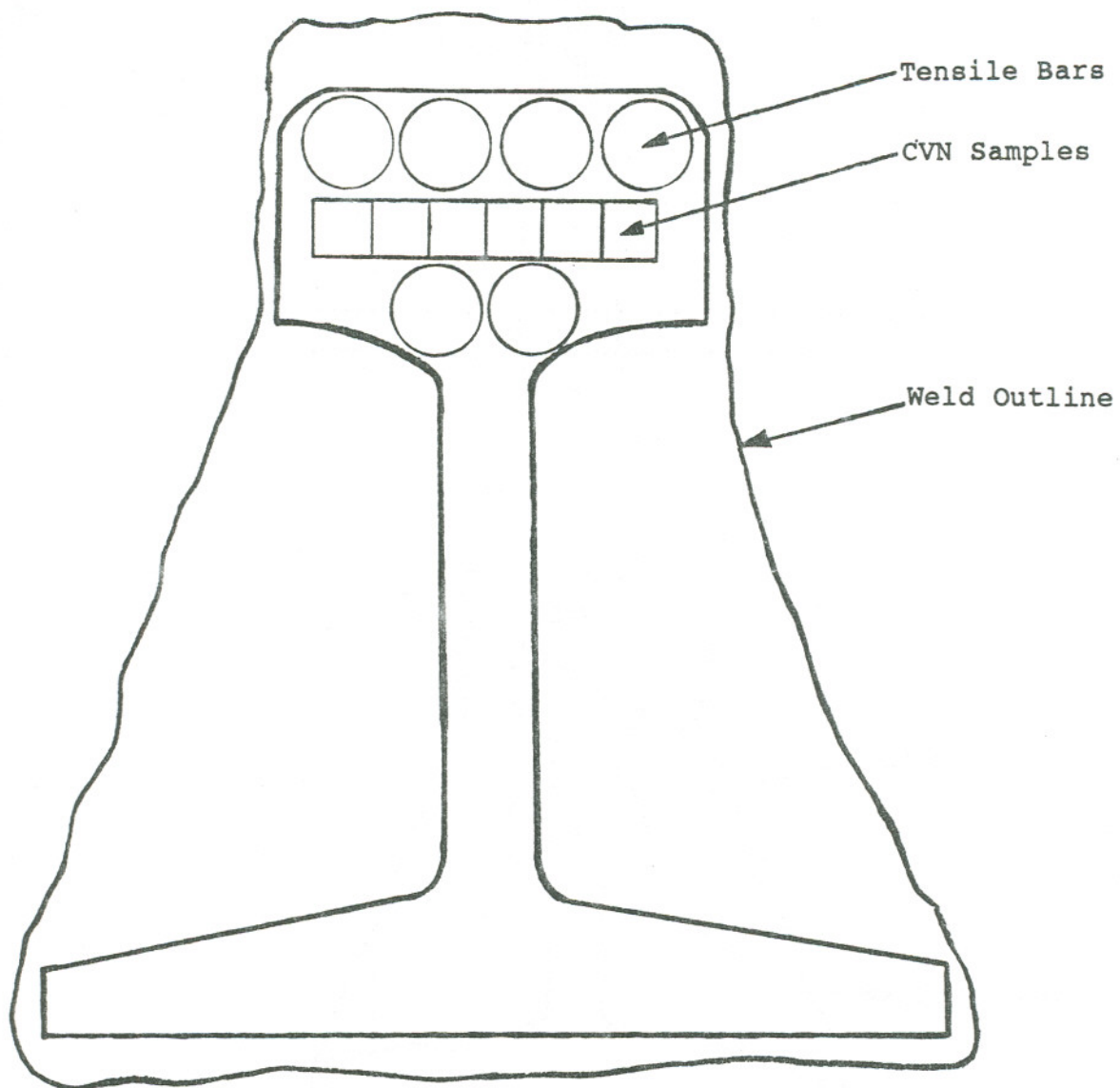
Figure 14. Electroslag Rail Weld Sample Placement
Tensile and Standard Charpy Bars

Longitudinal

Weld Outline

35mm

Weld Outline

Transverse
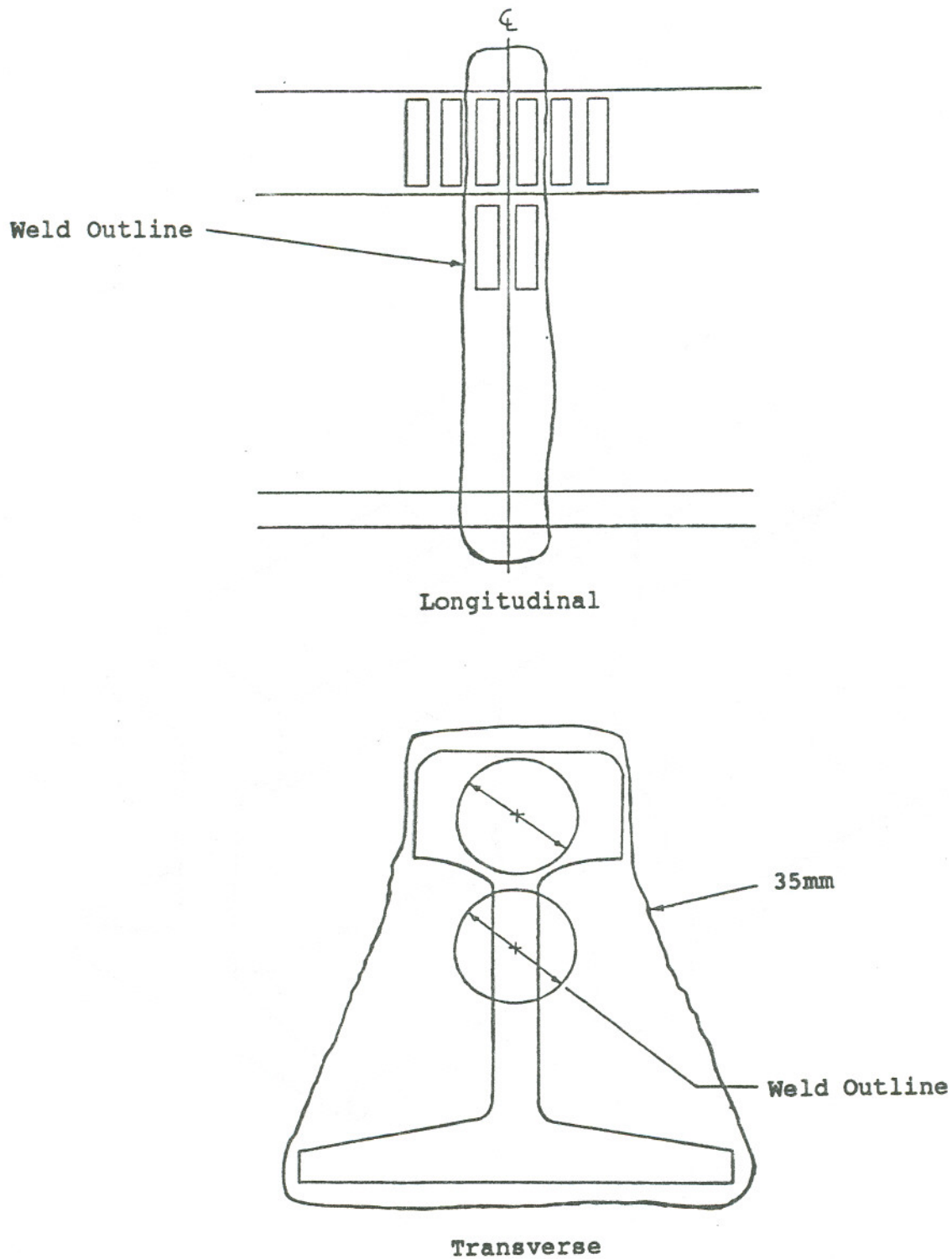
Figure 15. Electroslag Rail Weld Sample Placement
Amsler Wear and RCF Rollers
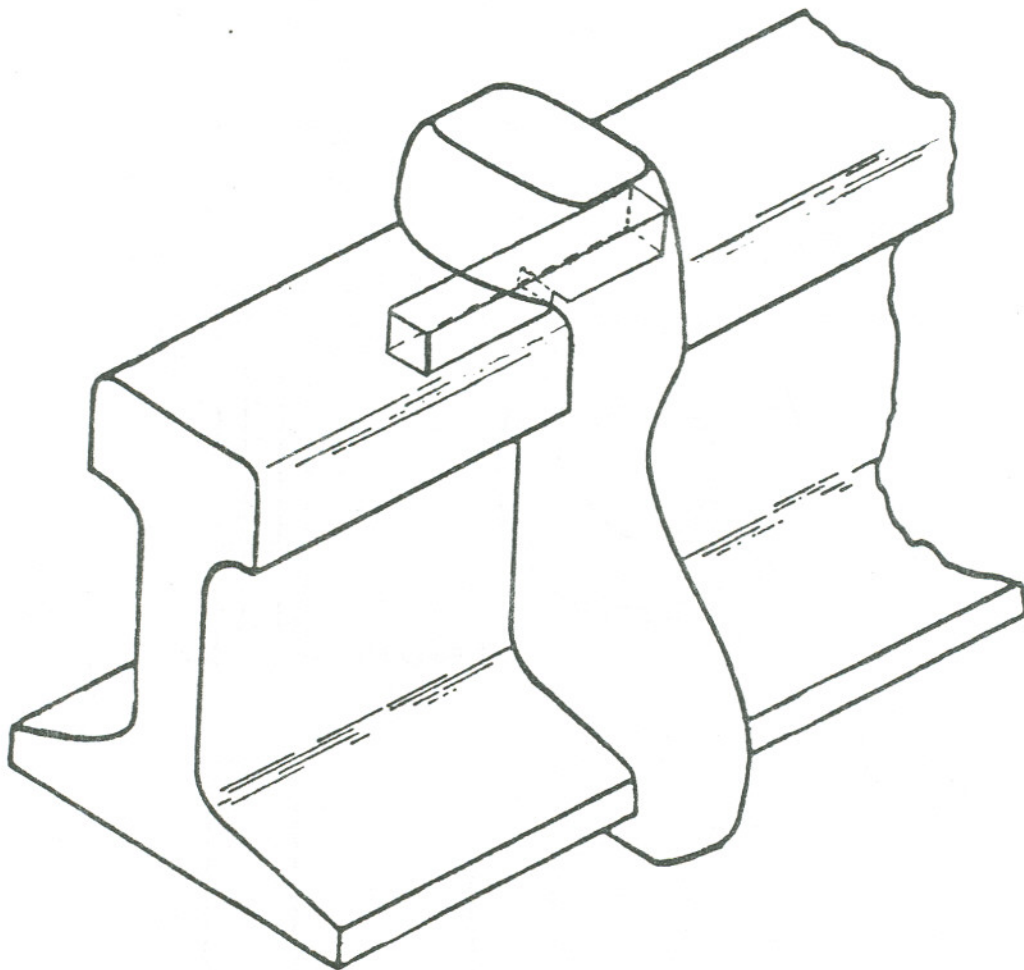
Figure 16. Orientation of Electroslag Rail Weld Charpy Samples

WEAR ROLLERS dimensions in inches (mm)

.394 (10.0)

.197 (5.0)

.197 (5.0)

.630 (16.0)
1.00 (25.0) top roller
1.384 (35.15) bottom roller
1.378 (35.00) top
1.778 (45.15) bottom

RCF ROLLERS

.157 (4.0)

30°   30°

.394 (10.0)

1.378 (35.00)

.630 (16.00)

1.778 (45,15)

.630 (16.0)

.394 (10.0)
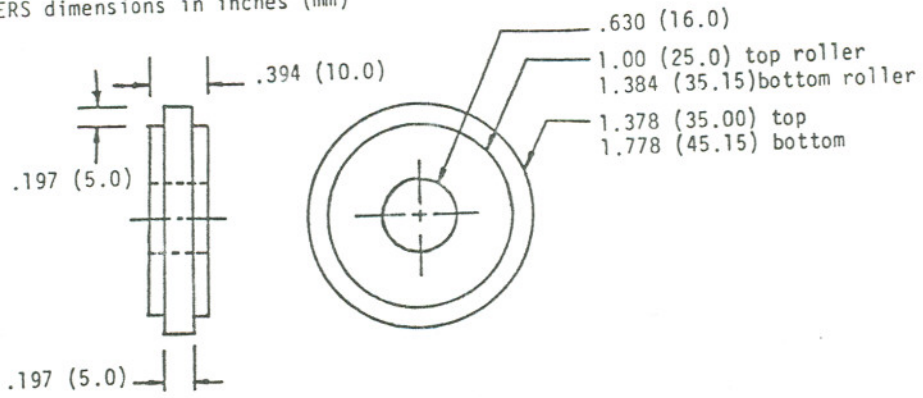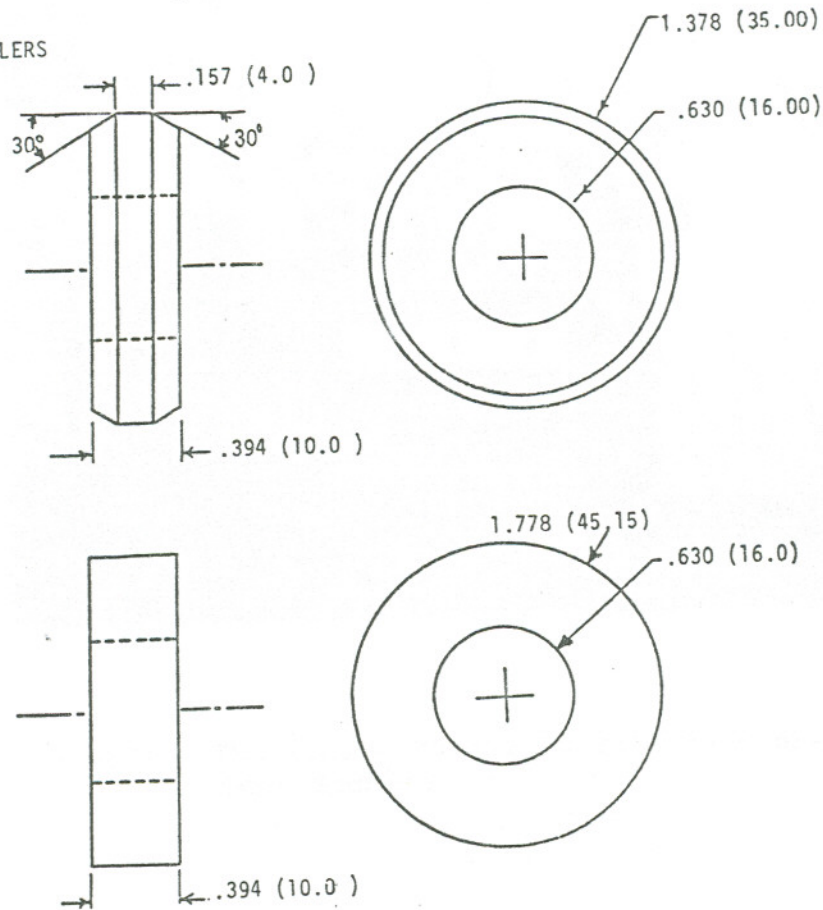
Figure 17. Machine Drawings of Amsler Rollers
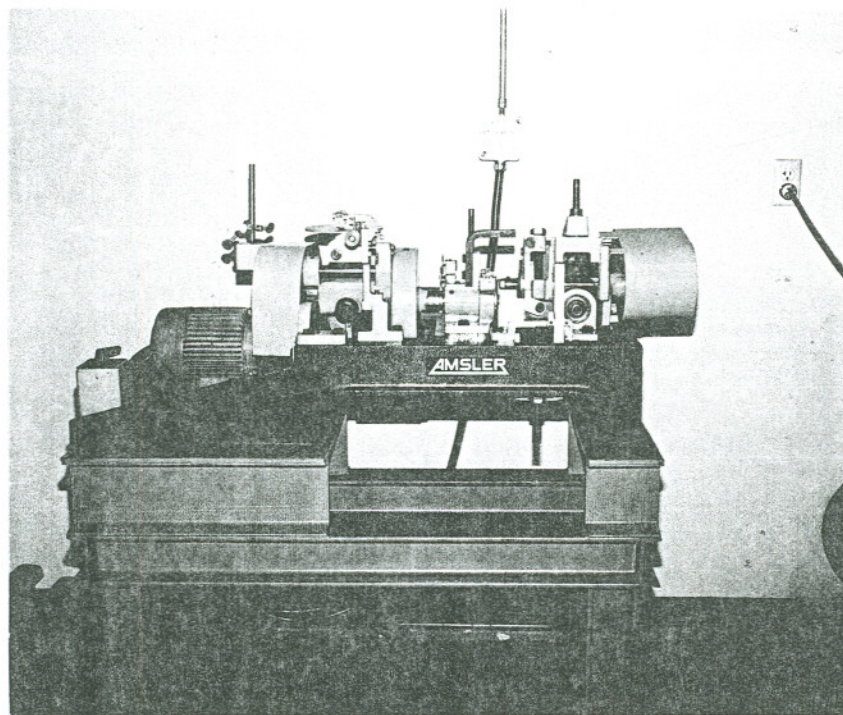
Figure 18. The Amsler Twin-Disk Rolling Contact
Test Machine
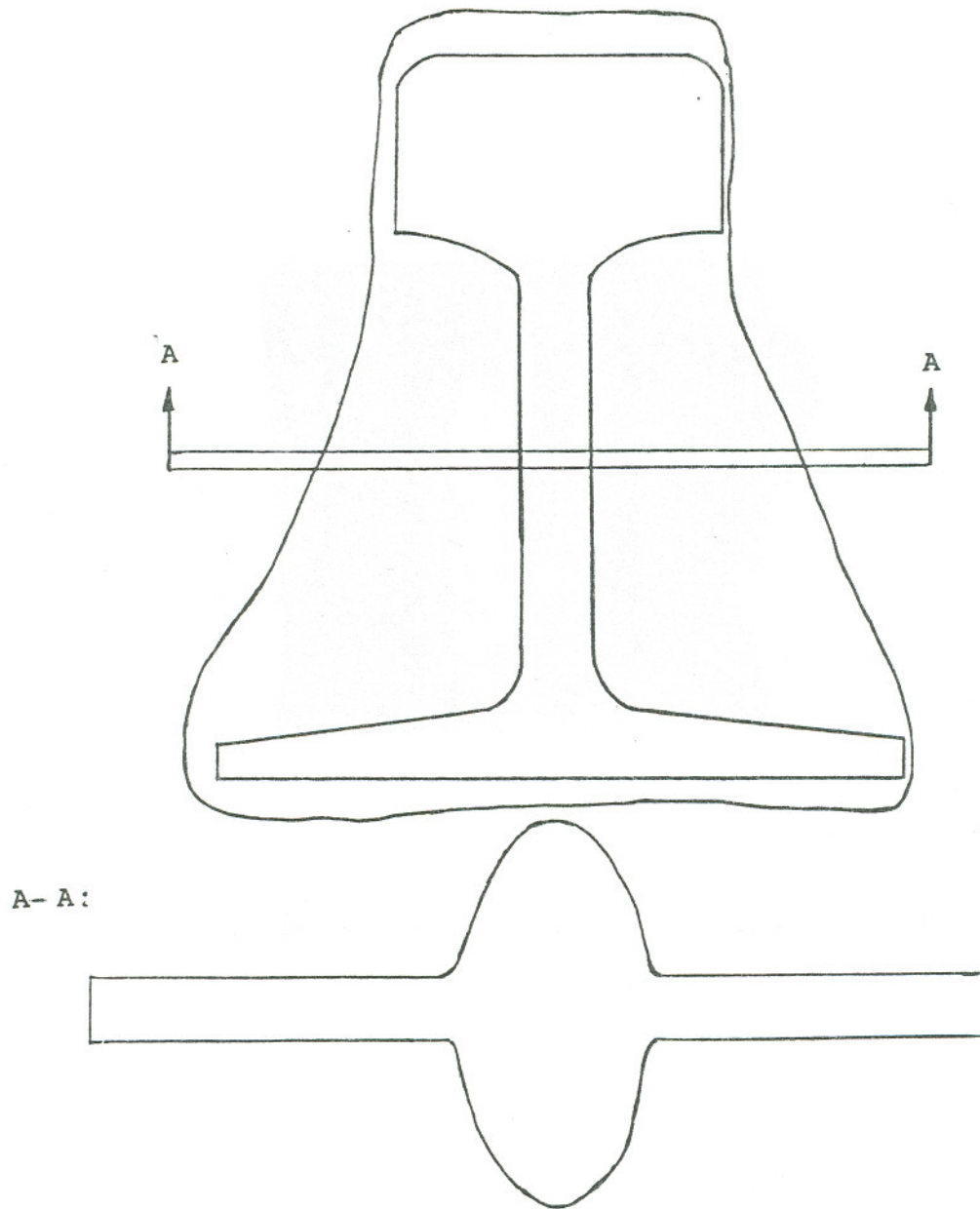
Figure 19. Electroslag Rail Weld Heat-Affected Zone Sectioning
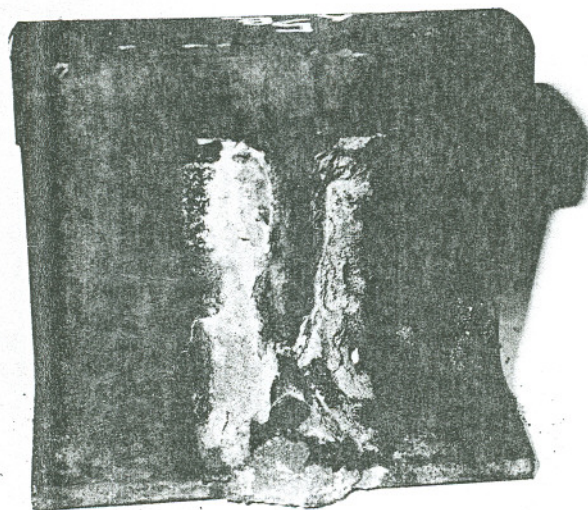
Figure 20. Mold Material on Thermite Weld
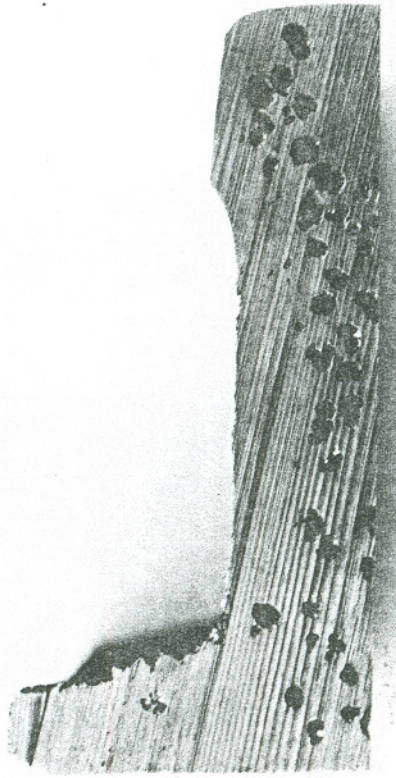
Transverse Section   Void Interior (100X)

Figure 21. Thermite Weld TW-6

Defect in
Weld Collar

Weld Outline
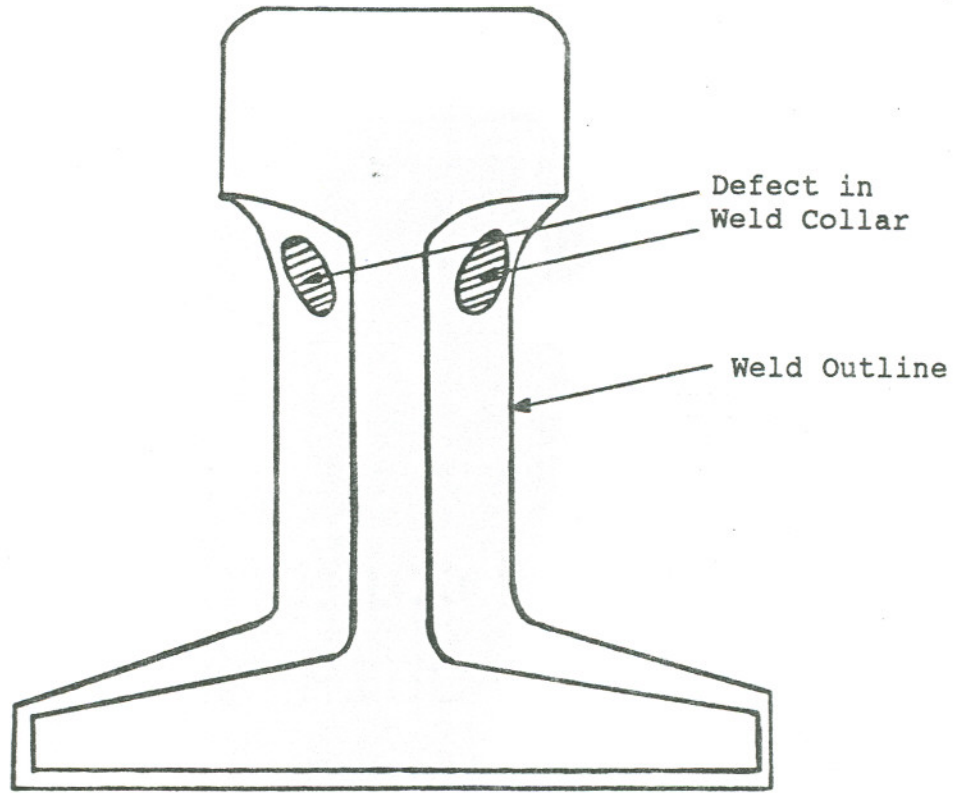
Transverse Section

Figure 22. Locations of Defects in Thermite Weld TW-2
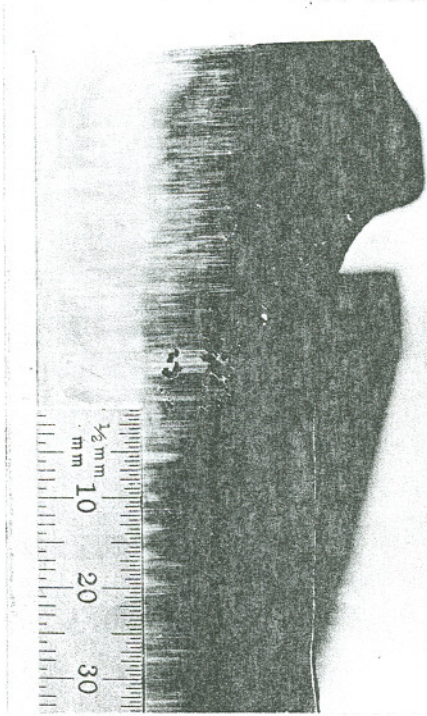
Figure 23. Macrophoto of Thermite Weld TW-2 Defect
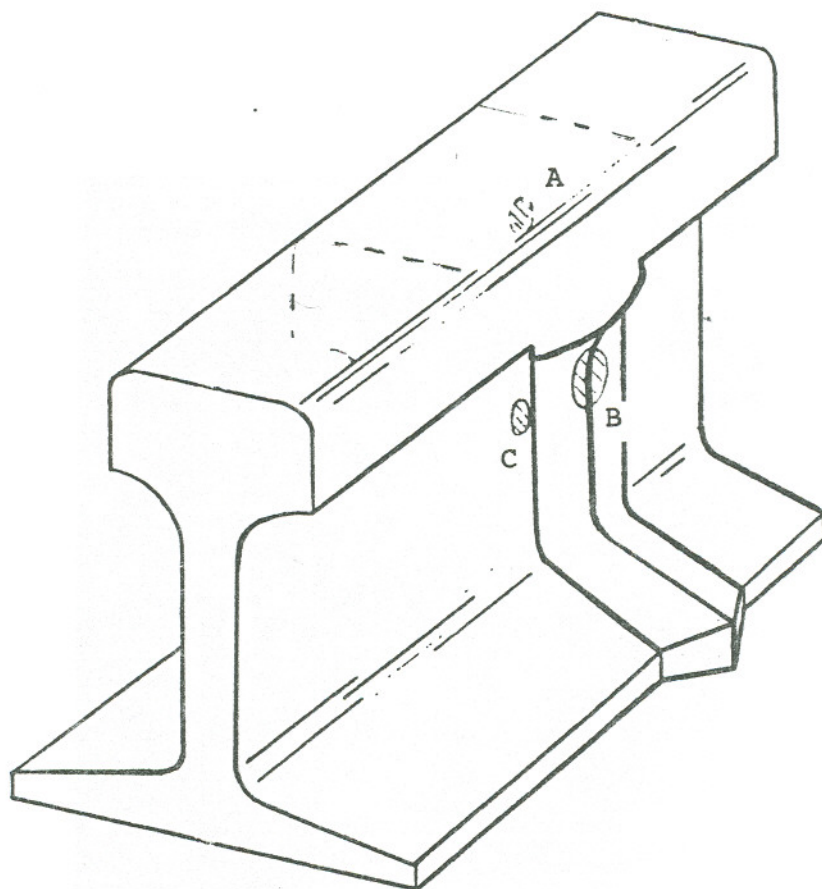
D (analogous to B on
hidden side of weld)

Figure 24. Locations of Defects in Thermite Weld TW-1
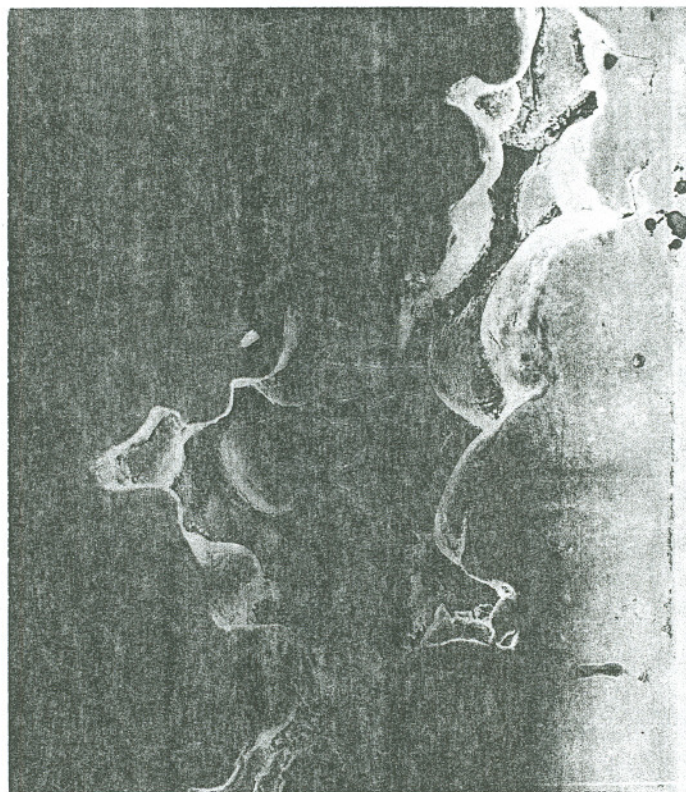
Figure 25. Dendrites in Collar Defect of
Thermite Weld TW-1 (220X)
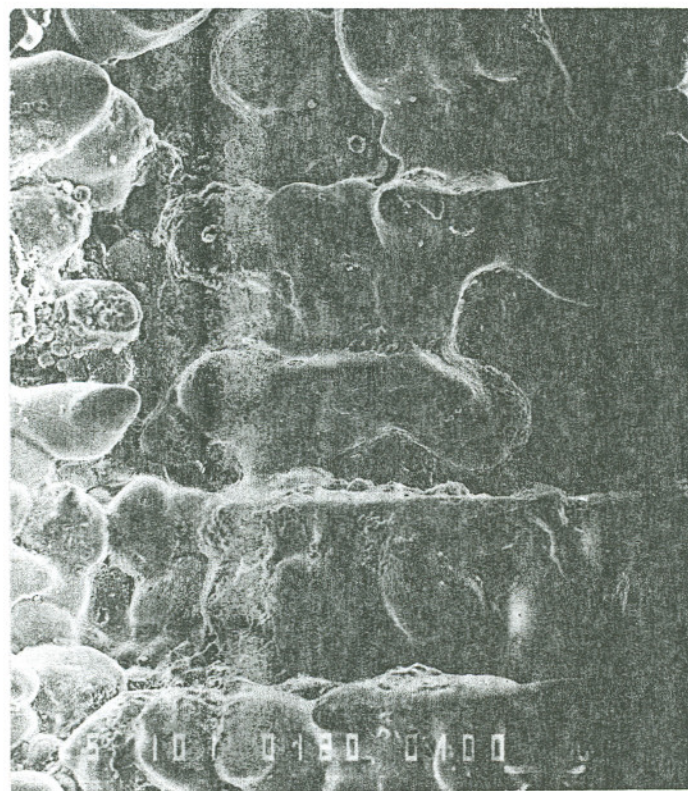
Figure 26. Dendrites in Collar Defect of
Thermite Weld TW-2 (100X)

Figure 27. Dendrites in Collar Defect of
Thermite Weld TW-3 (100X)

Figure 28. Dendrites in Collar Defect of
Thermite Weld TW-4 (100X)

Figure 29. Dendrites in Collar Defect of
Thermite Weld TW-5 (100X)
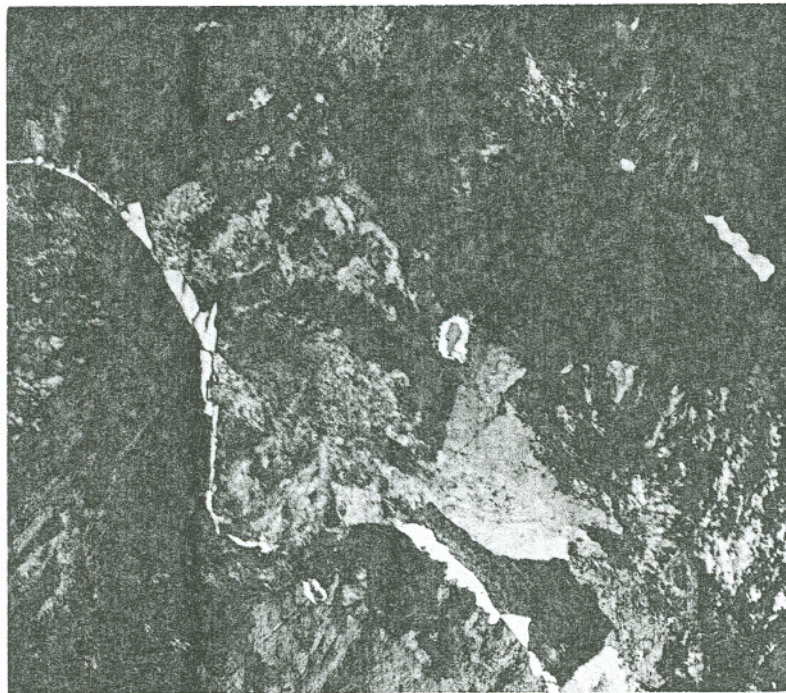
Figure 30. Typical Micrograph of
Thermite Weld TW-1 (400X)

Figure 31. Typical Micrograph of
Thermite Weld TW-2 (400)
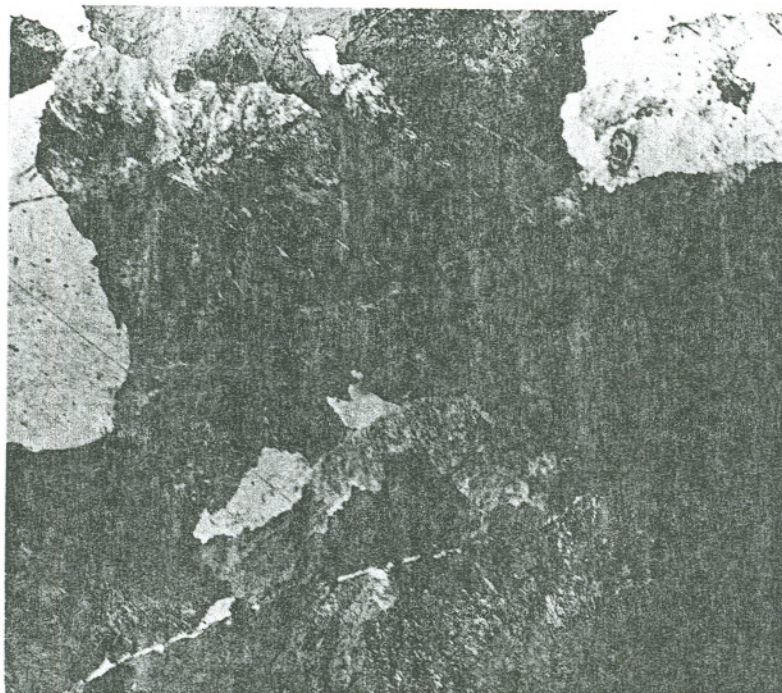
Figure 32. Typical Micrograph of
Thermite Weld TW-3 (400X)

Figure 33. Typical Micrograph of
Thermite Weld TW-4 (400X)

Figure 34. Typical Micrograph of
            of Thermite Weld TW-5 (400X)
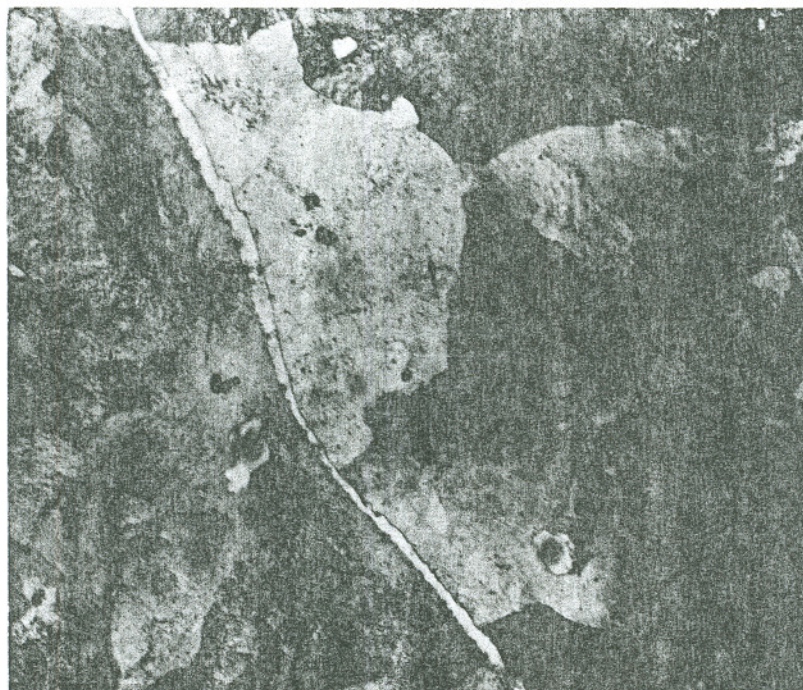
Figure 35. Typical Micrograph of
Thermite Weld TW-6 (400X)

Figure 36. Electroslag Rail Weld ES-1
Charpy Fracture Surface (150X)
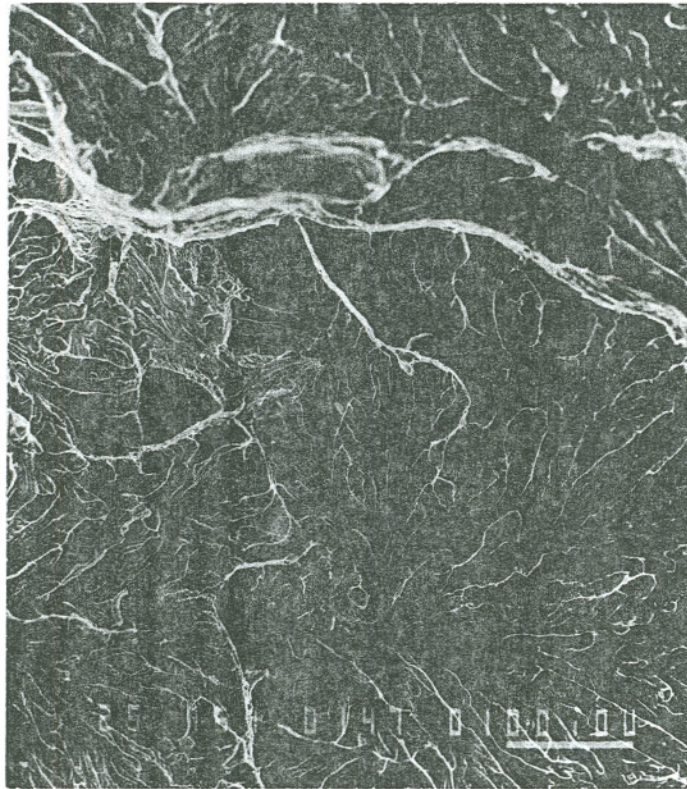
Figure 37. Electroslag Rail Weld ES-2
         Charpy Fracture Surface (150X)
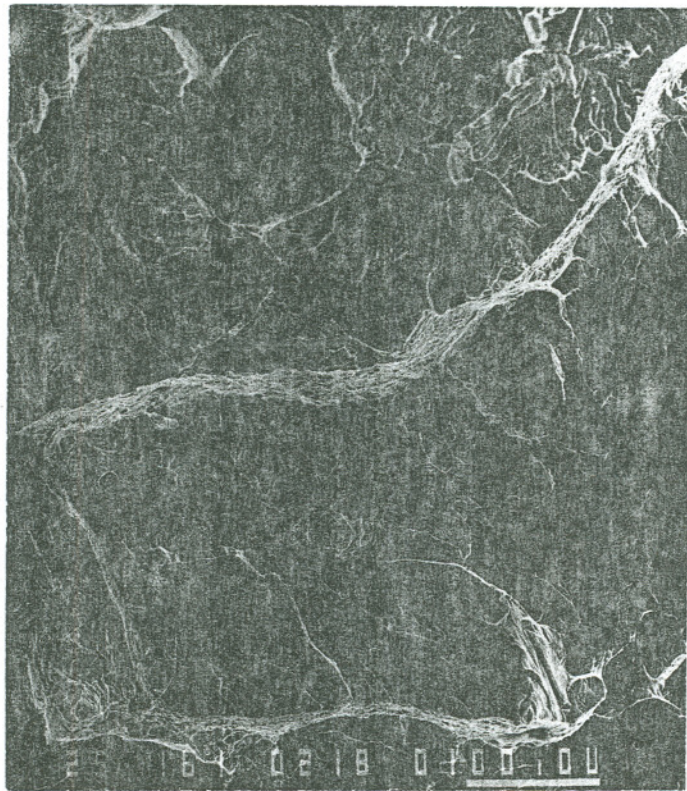
Figure 38. Electroslag Rail Weld ES-4
Charpy Fracture Surface (160X)

Figure 39. Electroslag Rail Weld ES-5
Charpy Fracture Surface (150X)
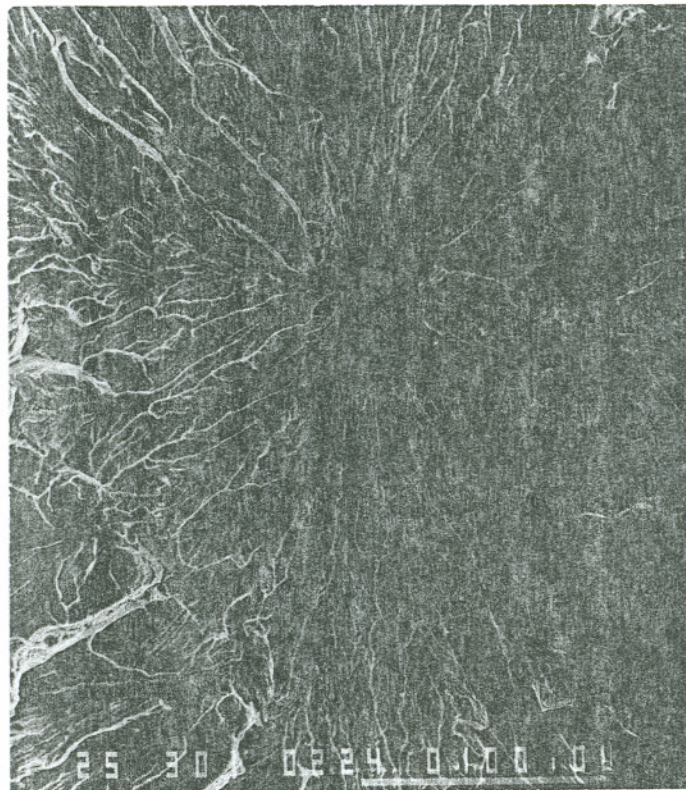
Figure 40. Fracture Initiation Site at Inclusion (300X)
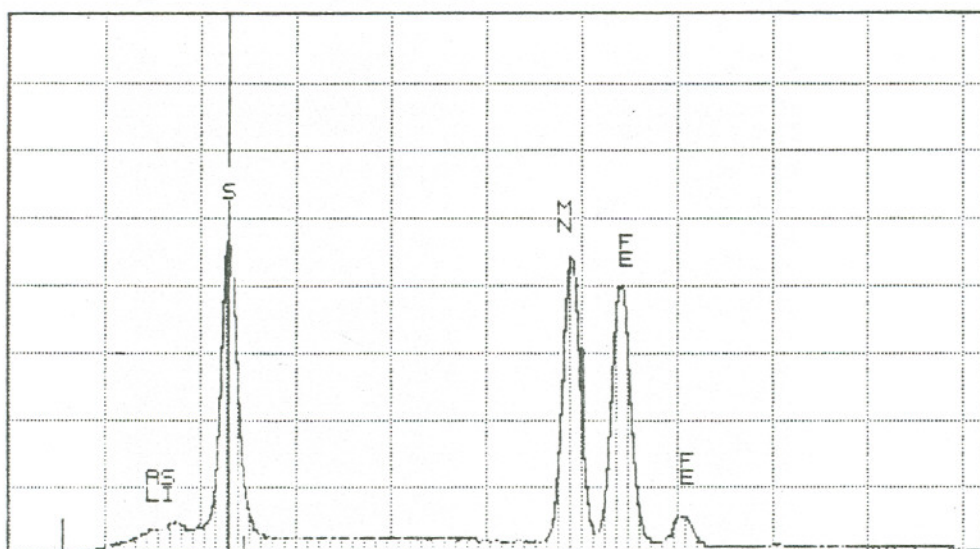
Figure 41. Energy Dispersive X-Ray Analysis of MnS Inclusion

Figure 42. Electroslag Rail Weld ES-1
Tensile Failure Surface (150X)

Figure 43. Electroslag Rail Weld ES-2
          Tensile Failure Surface (200X)

Figure 44. Electroslag Rail Weld ES-4
Tensile Failure Surface (180X)
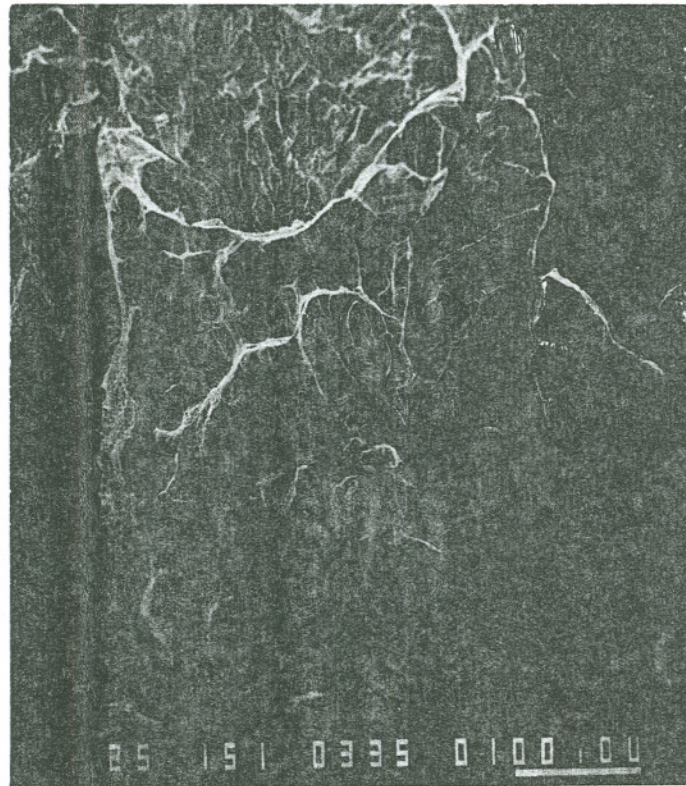
Figure 45. Electroslag Rail Weld ES-5
           Tensile Failure Surface (150)
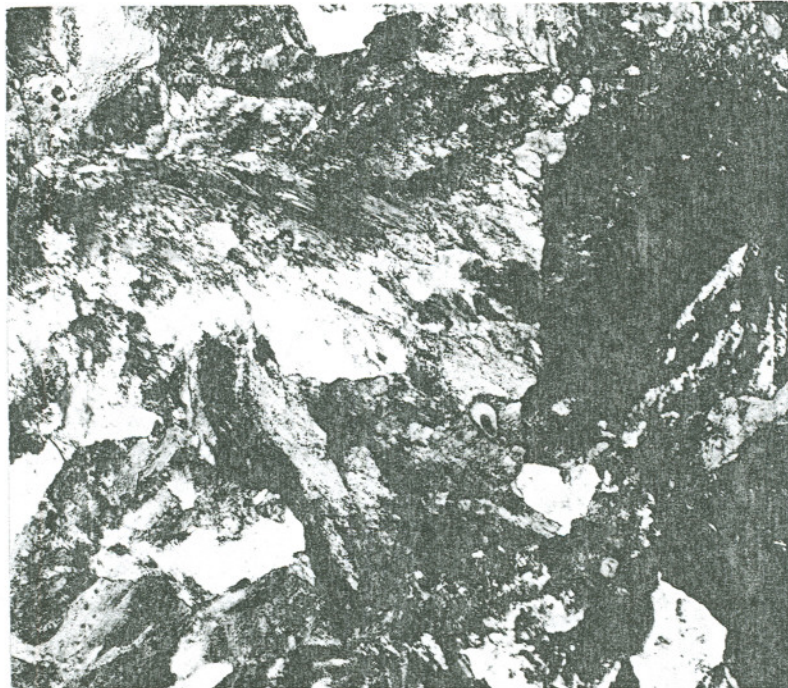
Figure 46. Typical Micrograph of
Electroslag Weld ES-1 (400X)
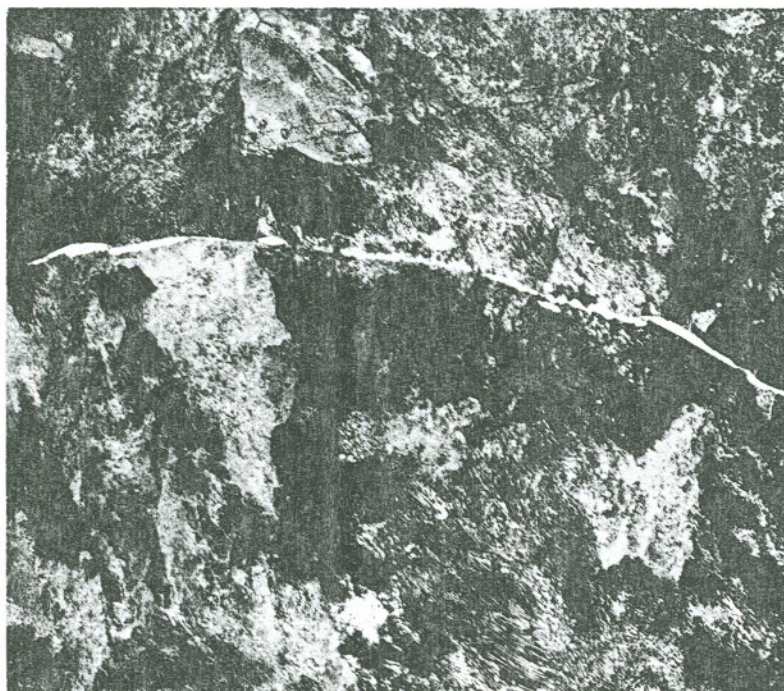
Figure 47. Typical Micrograph of
Electroslag Weld ES-2 (400X)

Figure 48. Typical Micrograph of
Electroslag Weld ES-3 (400X)
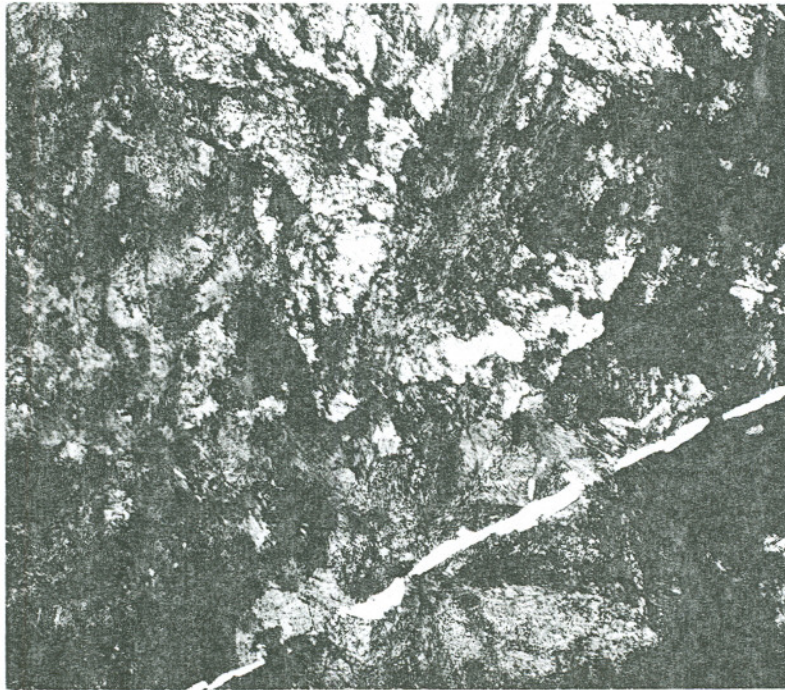
Figure 49. Typical Micrograph of
Electroslag Weld ES-4 (400X)
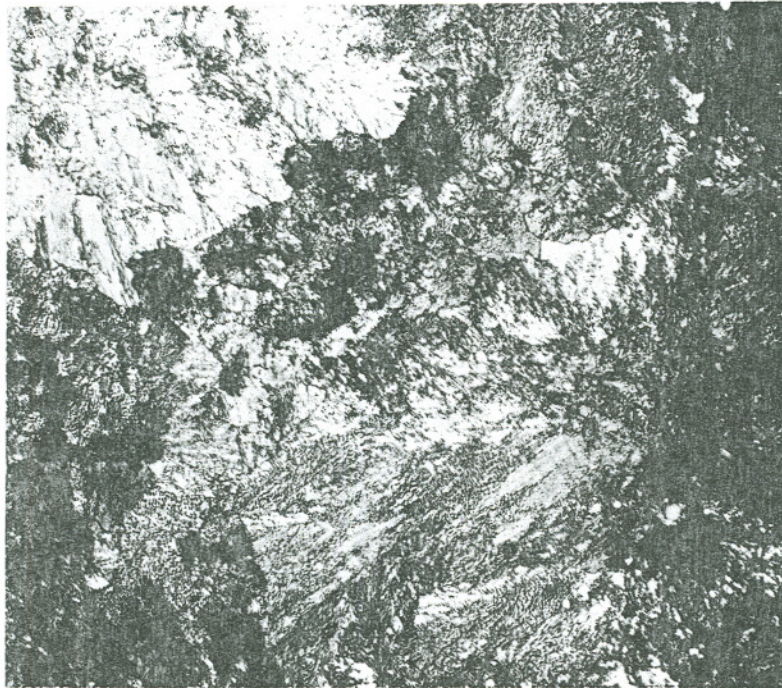
Figure 50. Typical Micrograph of
Electroslag Weld ES-5 (400X)

Figure 51. Typical Micrograph of
Electroslag Weld ES-6 (400X)
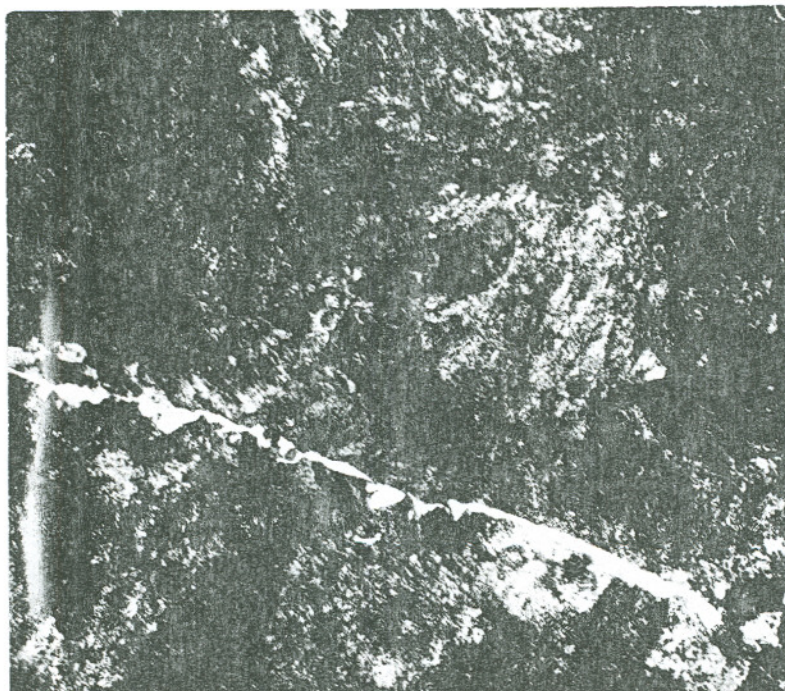
Figure 52. Typical Micrograph of
Electroslag Weld ES-7 (400X)

Figure 53. Typical Micrograph of
Electroslag Weld ES-8 (400X)
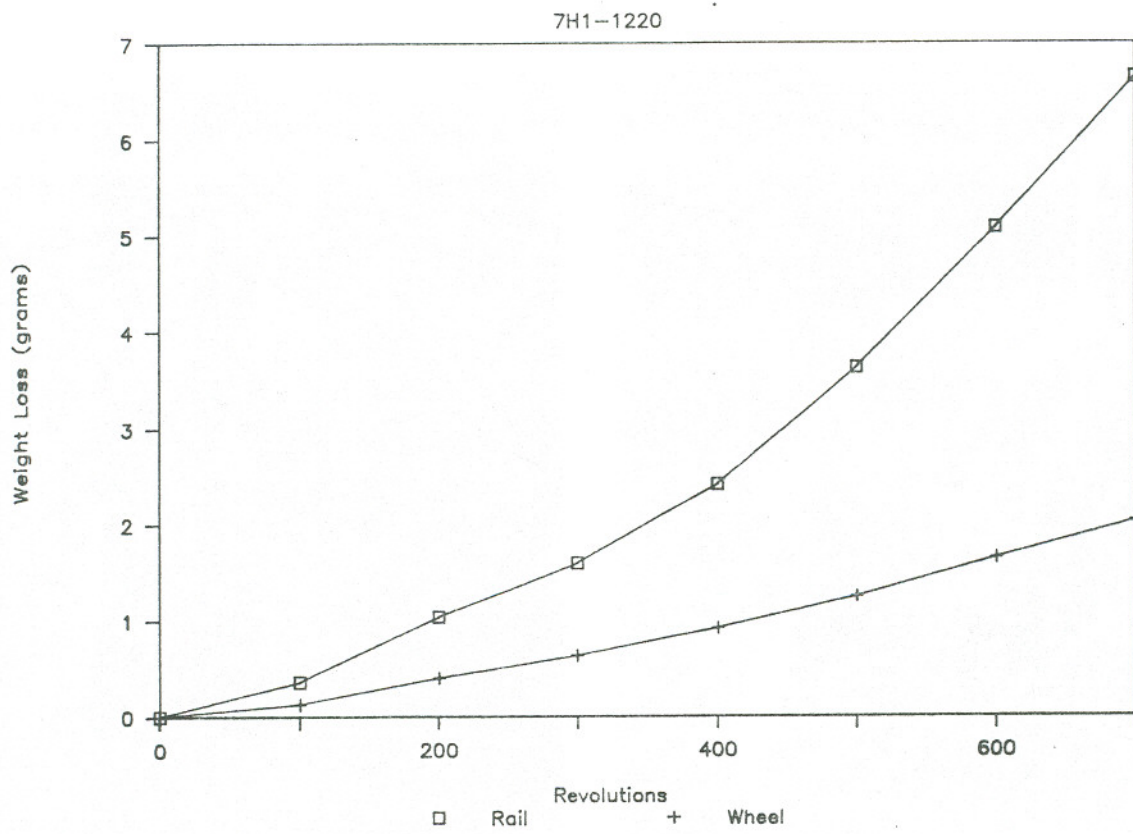
Figure 54. Example Weight Loss vs. Revolutions Curve
of Wear Test
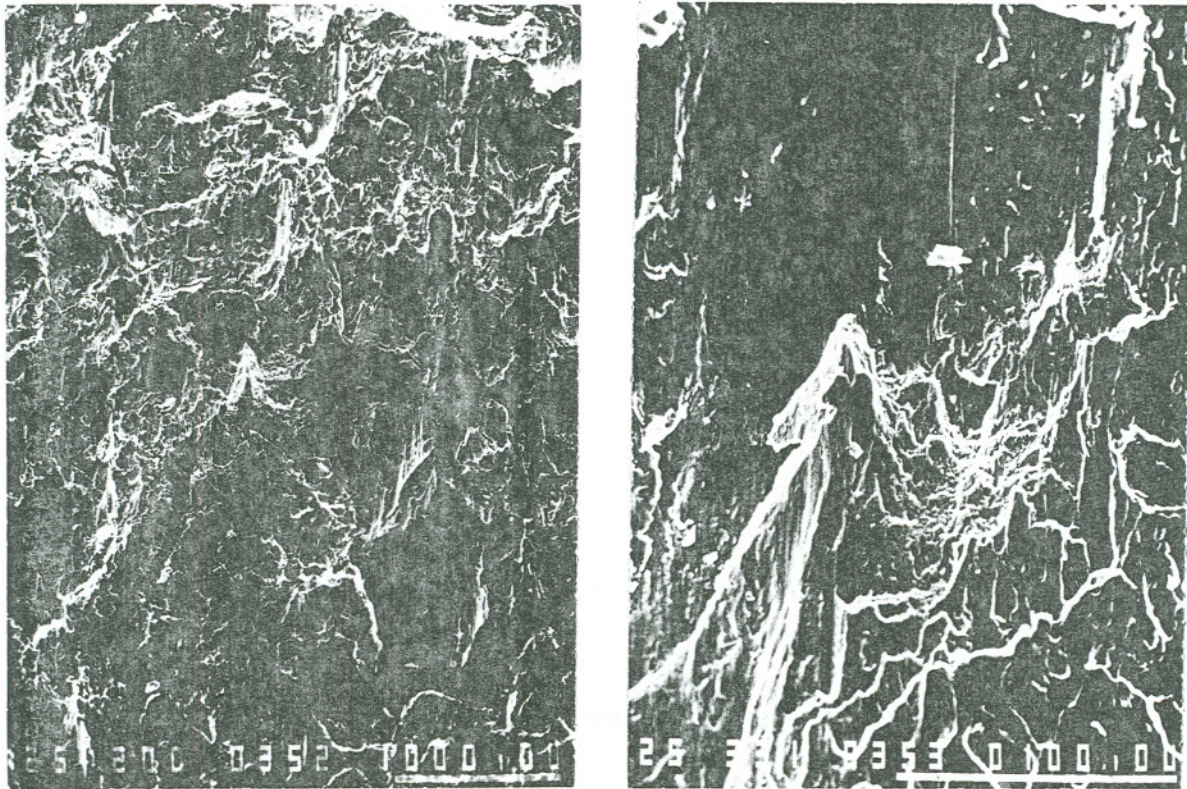
Figure 55. Type III Wear on Amsler Roller
(200X and 330X)
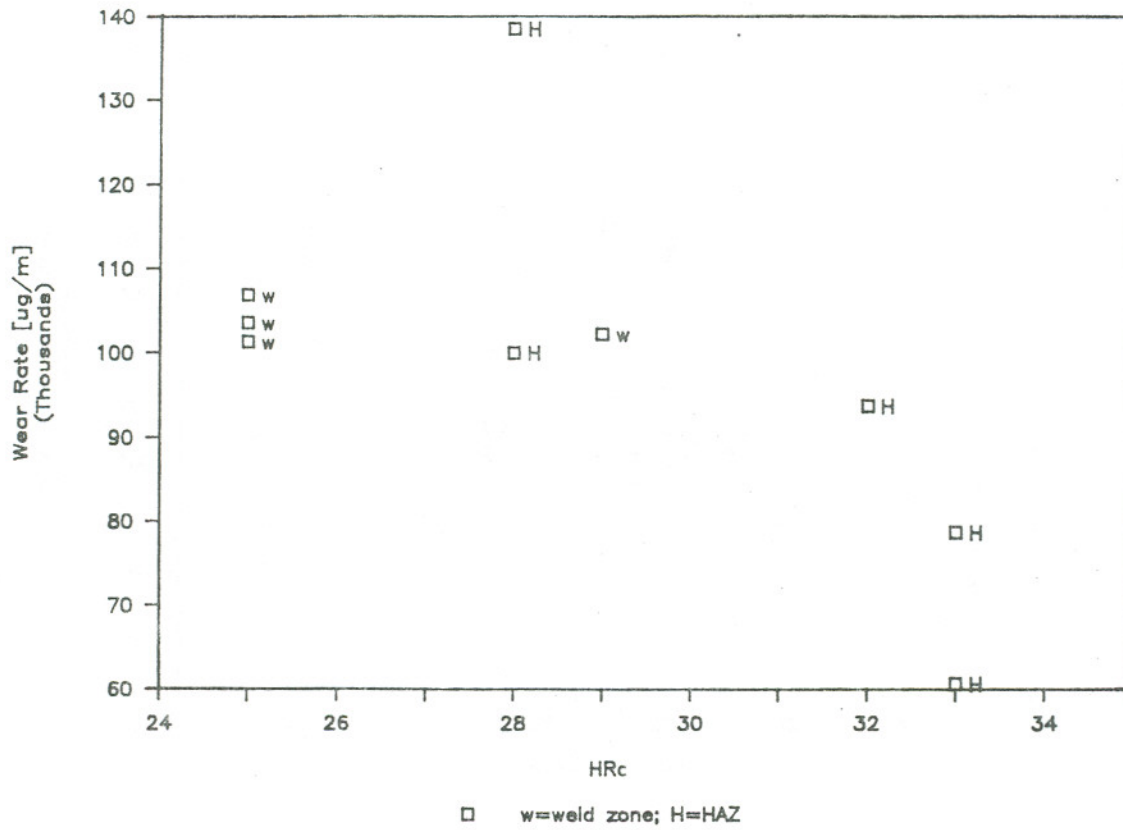
Figure 56. Wear Rate vs. Hardness at 1220 N/sq.mm
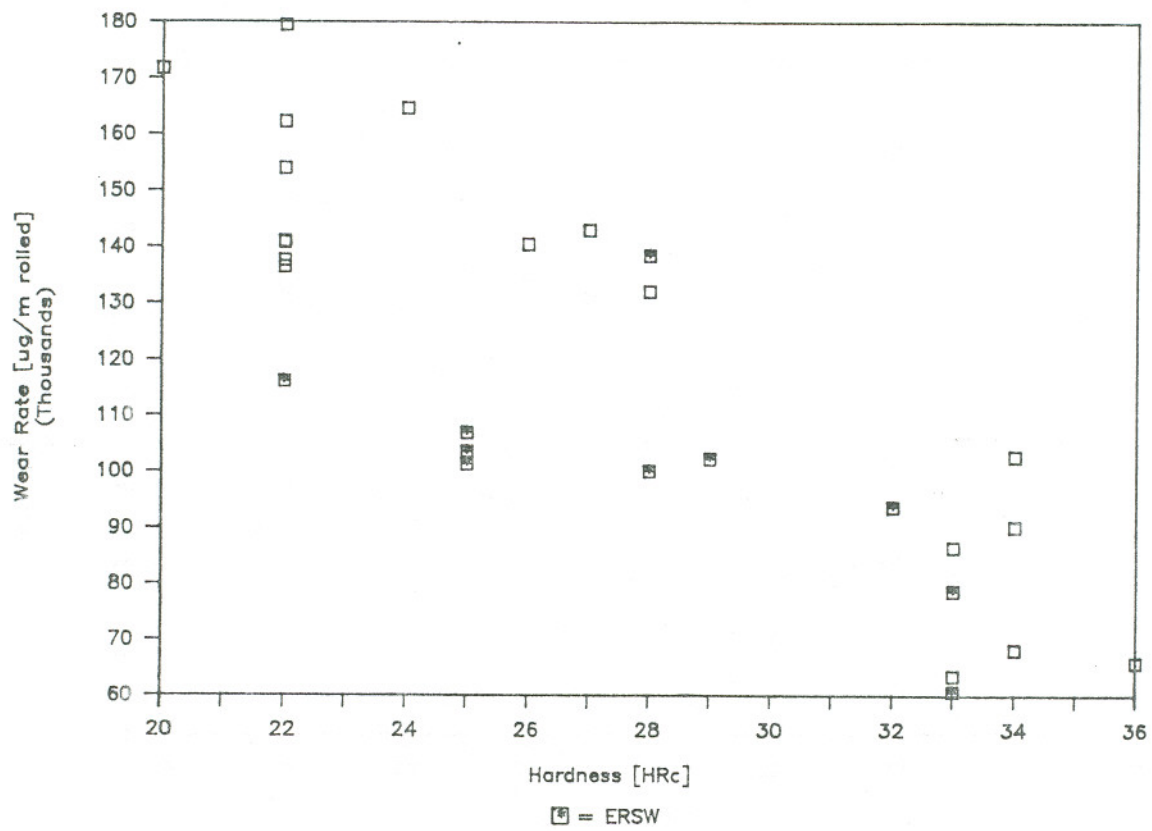
Figure 57. Wear Rate vs. Hardness at 1220 N/sq.mm
Combined Data
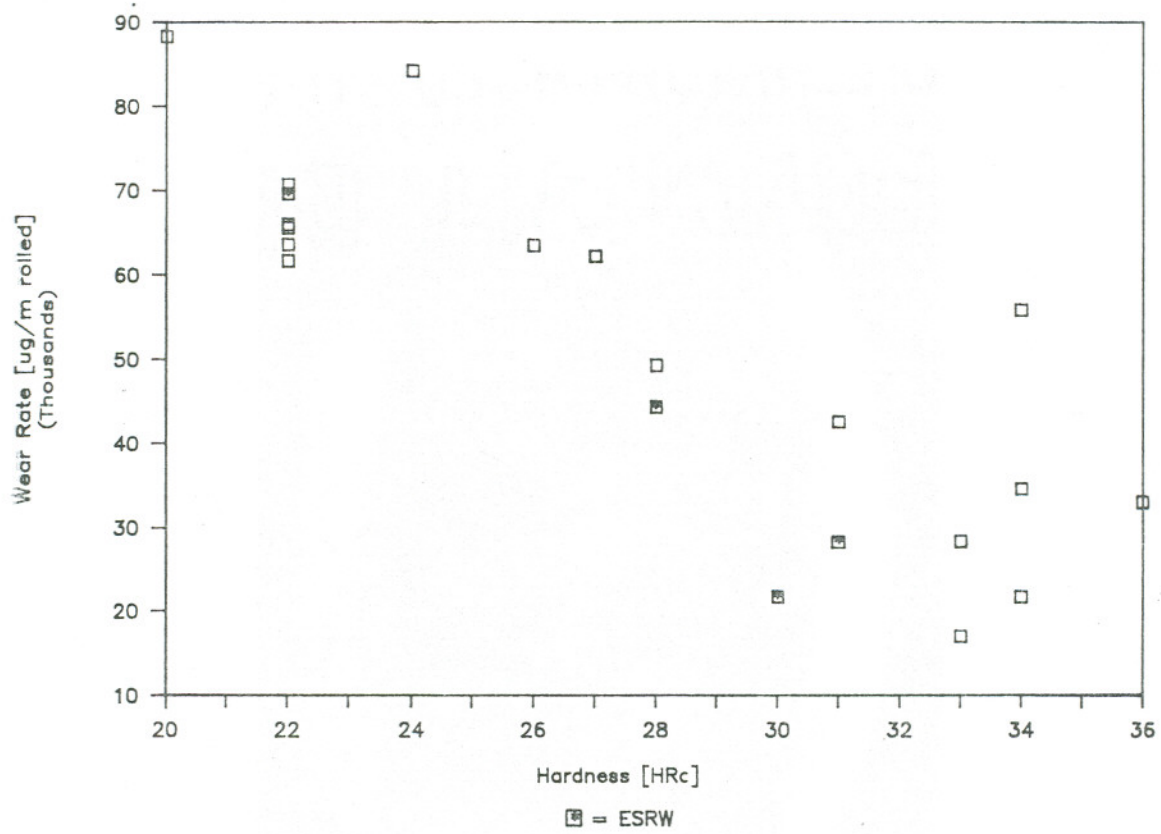
Figure 58. Wear Rate vs. Hardness at 900 N/sq.mm
Combined Data
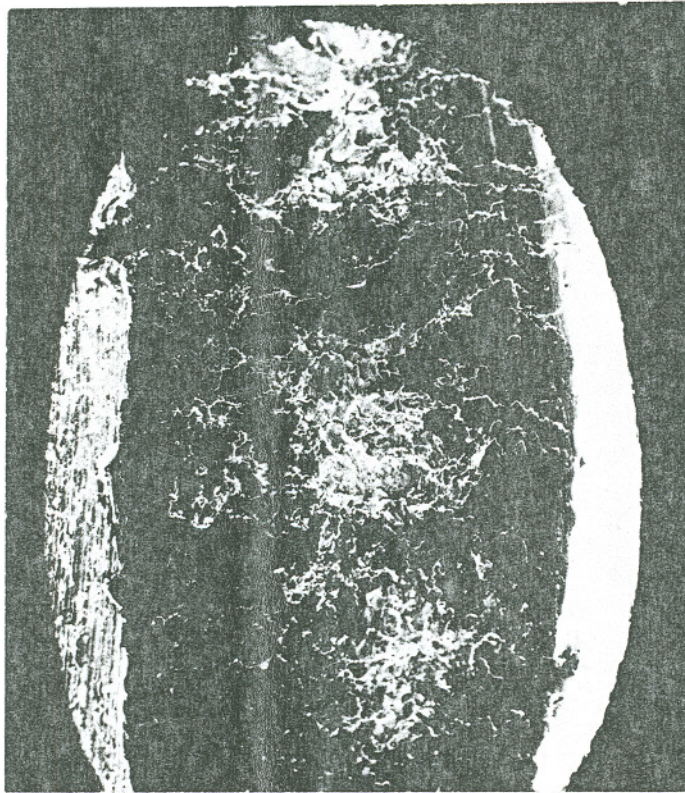
Figure 59. Rolling Contact Fatigue
Failure (10X)
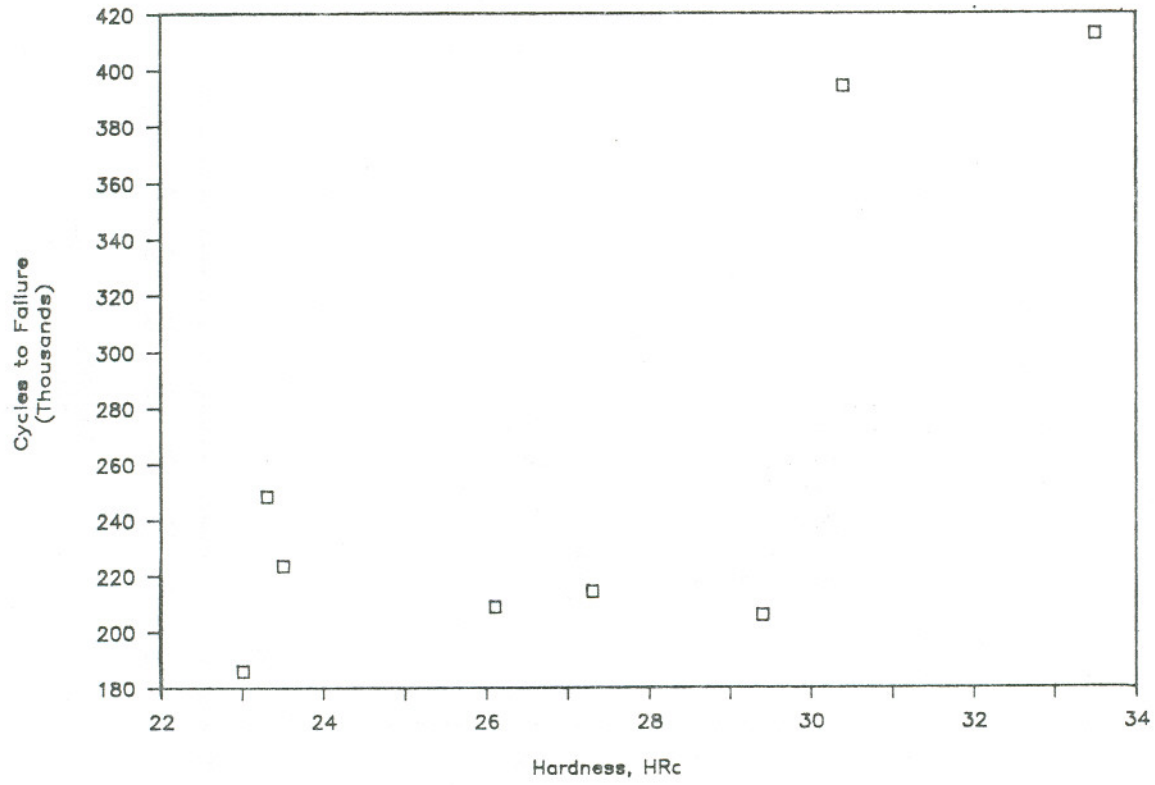
Figure 60. Rolling Contact Fatigue Life vs. Hardness
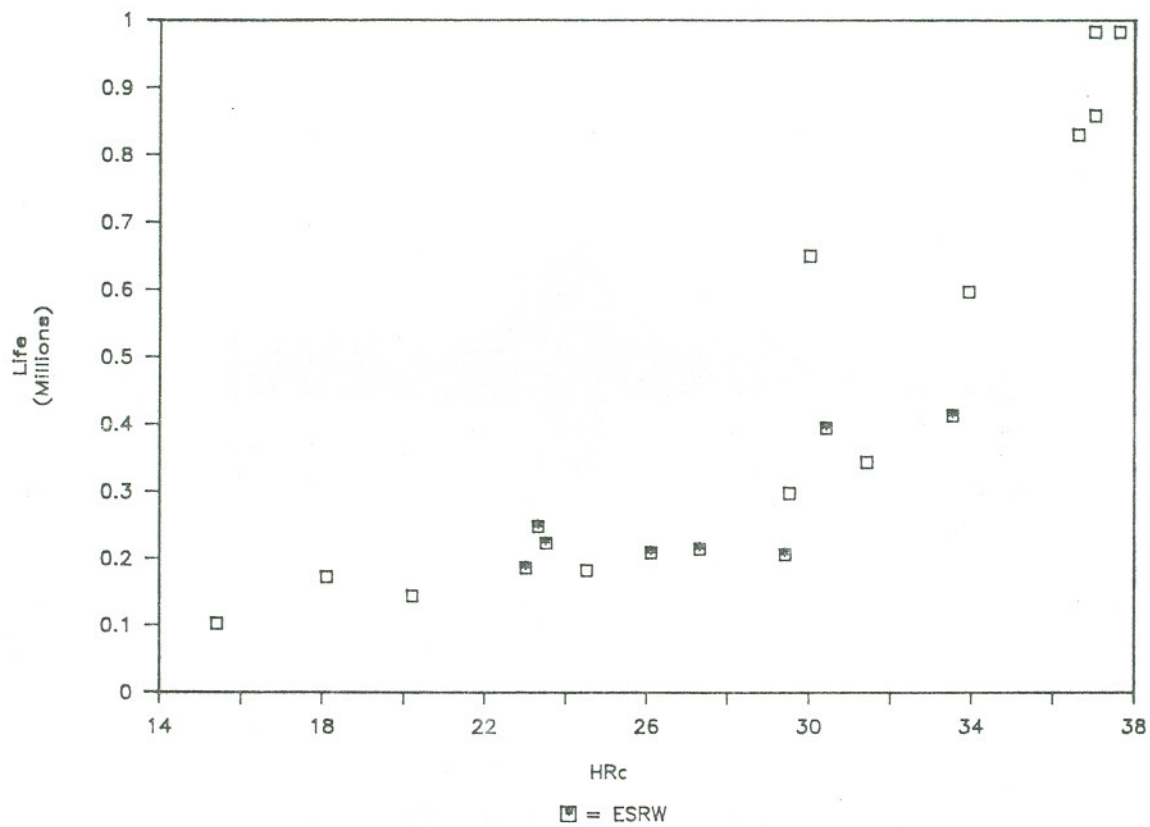
Figure 61. Rolling Contact Fatigue Life vs. Hardness
Combined Data
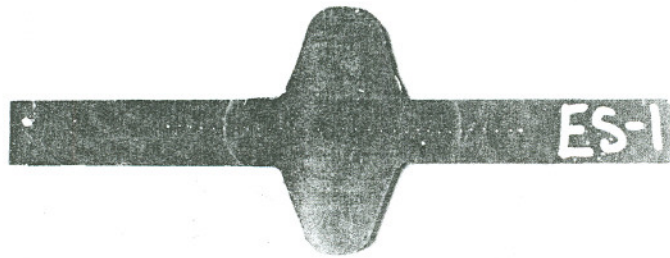
Figure 62. Heat-Affected Zone of
Electroslag Weld ES-1
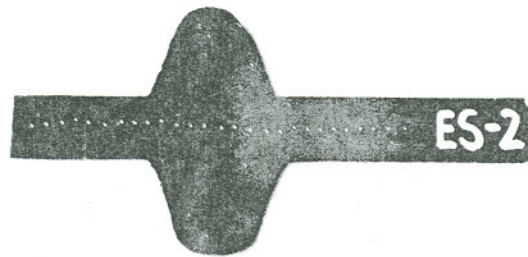
Figure 63. Heat-Affected Zone of
Electroslag Weld ES-2
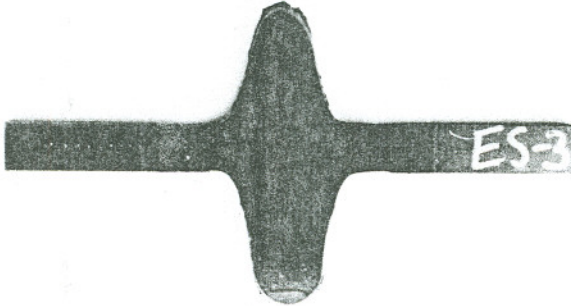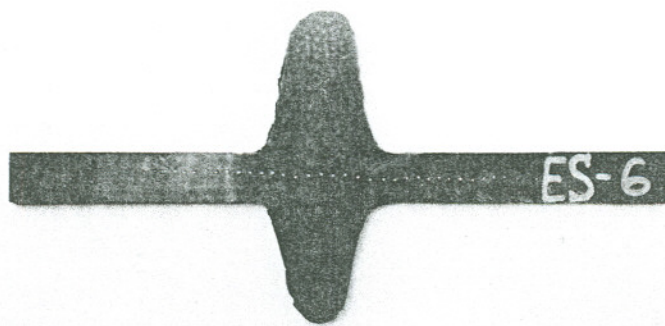
Figure 64. Heat-Affected Zone of
Electroslag Weld ES-3
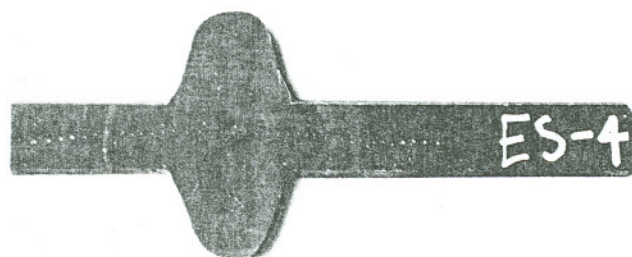
Figure 65. Heat-Affected Zone of
Electroslag Weld ES-4
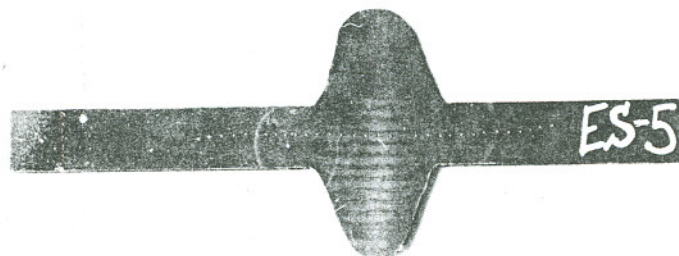
Figure 66. Heat-Affected Zone of
Electroslag Weld ES-5

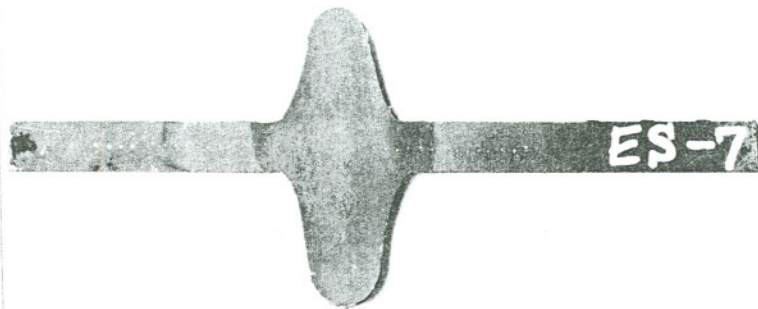Figure 67. Heat-Affected Zone of
Electroslag Weld ES-6

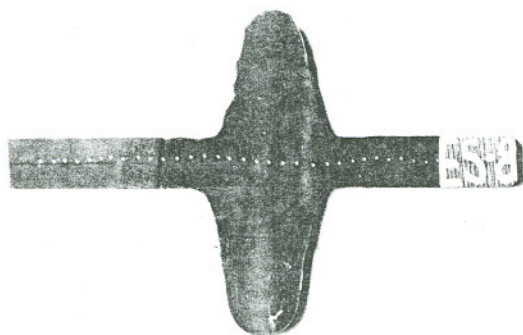Figure 68. Heat-Affected Zone of
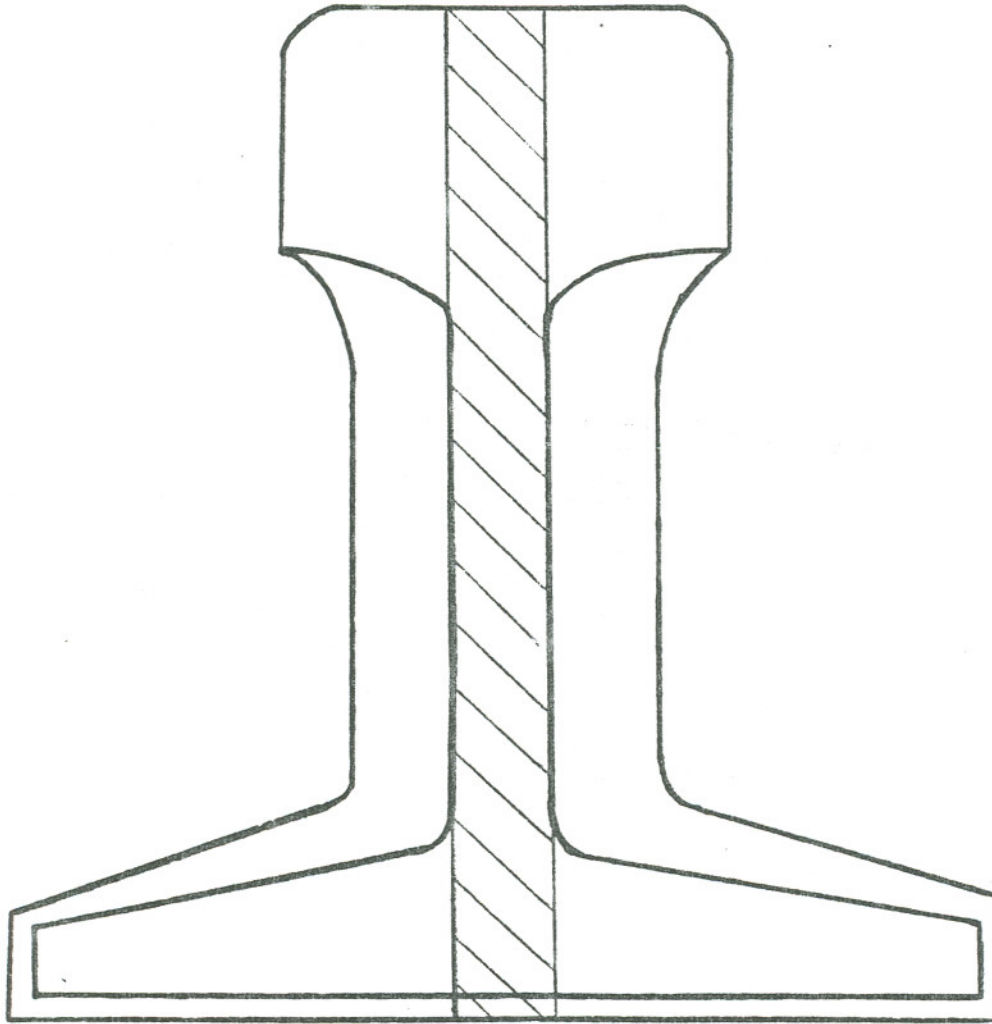Electroslag Weld ES-7

Figure 69. Heat-Affected Zone of
Electroslag Weld ES-8

Figure 70. Ultrasonic Scan of Rail Cross-Section